Fall 2009

Depth evaluation of damage to aircraft fuselage skins using microwave and millimeter wave methods

Andrew Dale McClanahan

Department:

Recommended Citation

McClanahan, Andrew Dale, "Depth evaluation of damage to aircraft fuselage skins using microwave and millimeter wave methods" (2009). *Masters Theses*. 7079.
https://scholarsmine.mst.edu/masters_theses/7079

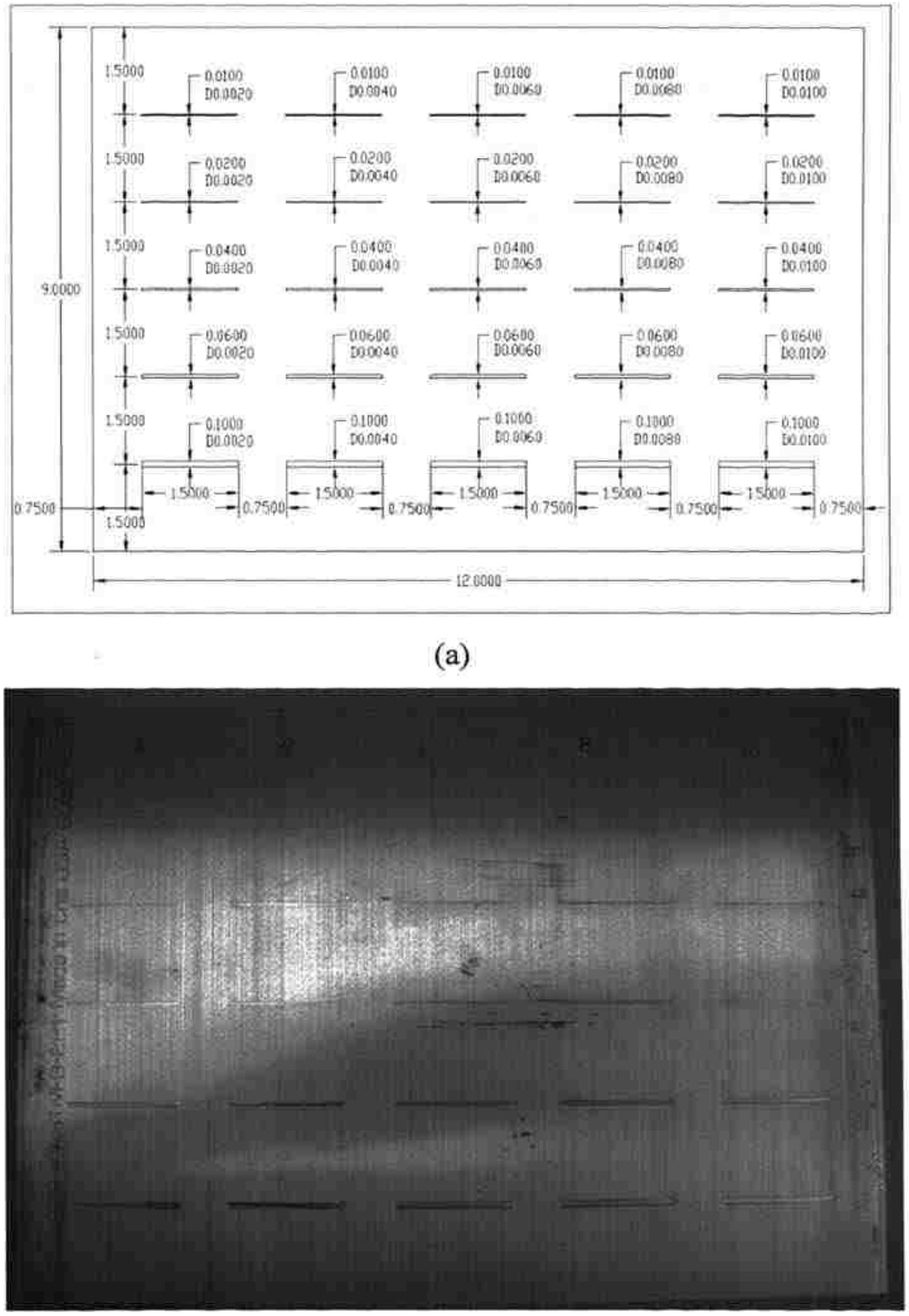

(a)

(b)

Figure 1.2. Shallow machined finite cracks sample: a) schematic and b) picture. In a), dimensions are in inches and "*D*" denotes the depth of the crack.

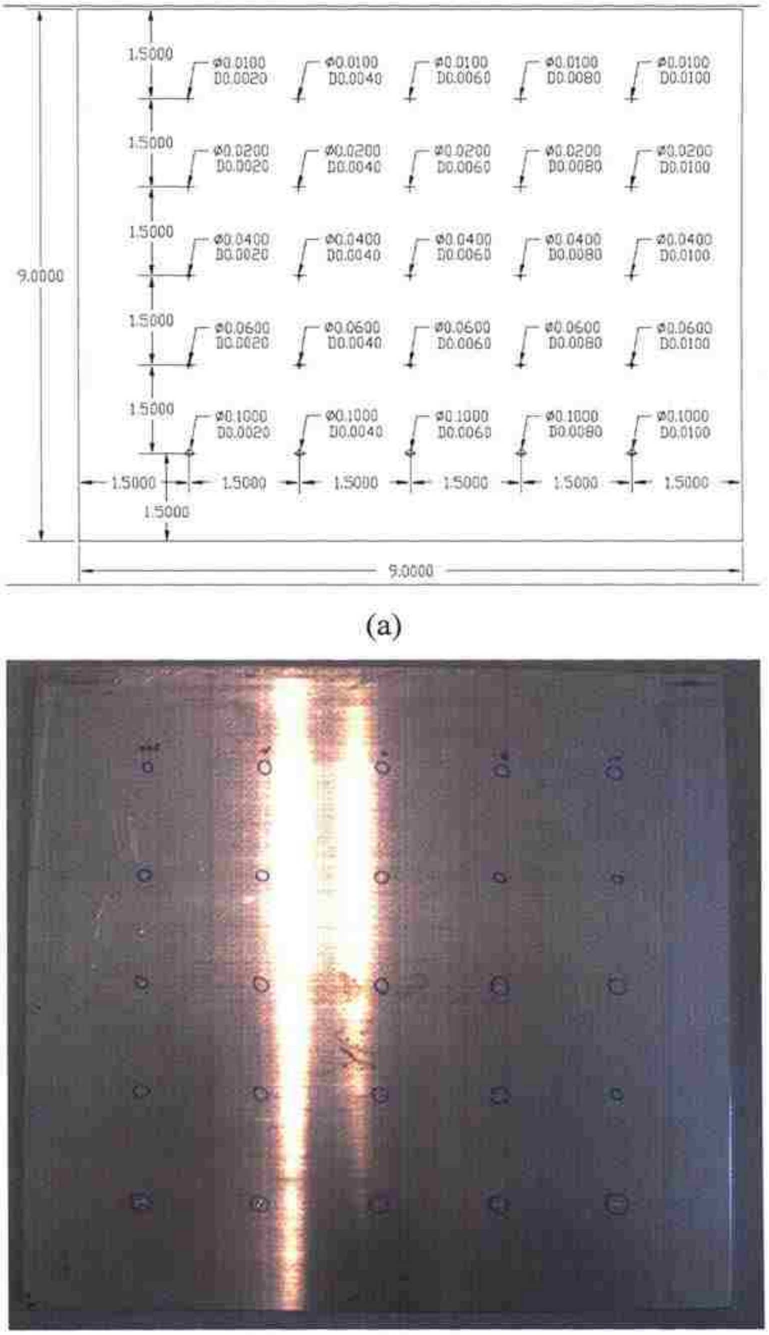

Figure 1.3. Shallow machined pits sample: a) schematic and b) picture. In a), dimensions are in inches and "*D*" denotes the depth of the pit.

Table 1.3. Actual pit widths and depths for shallow machined pit sample.

Desired Depth (mm) *Width (mm)*	0.05	0.10	0.15	0.20	0.25
0.25	0.06	0.13	0.19	0.19	0.27
0.51	0.08	0.14	0.21	0.25	0.17
1.02	0.05	0.13	0.26	0.24	0.25
1.52	0.07	0.16	0.19	0.23	0.26
2.54	0.07	0.14	0.22	0.26	0.25

The third plate was prepared using laser machining, and is shown in Figure 1.4. Figure 1.4a shows the schematic of this plate. Visual inspection under magnification showed that these pits had irregular bottoms. Two sets of forty eight pits were cut with diameters from 0.2-1.0 mm and desired depths from 0.15-0.4 mm. A picture of the final plate is shown in Figure 1.4b. Accurate readings with the micrometer could not be achieved for pits with diameters smaller than 0.5 mm on this sample, so the desired depths are used for these pits. The measured pit depths are given in Table 1.4.

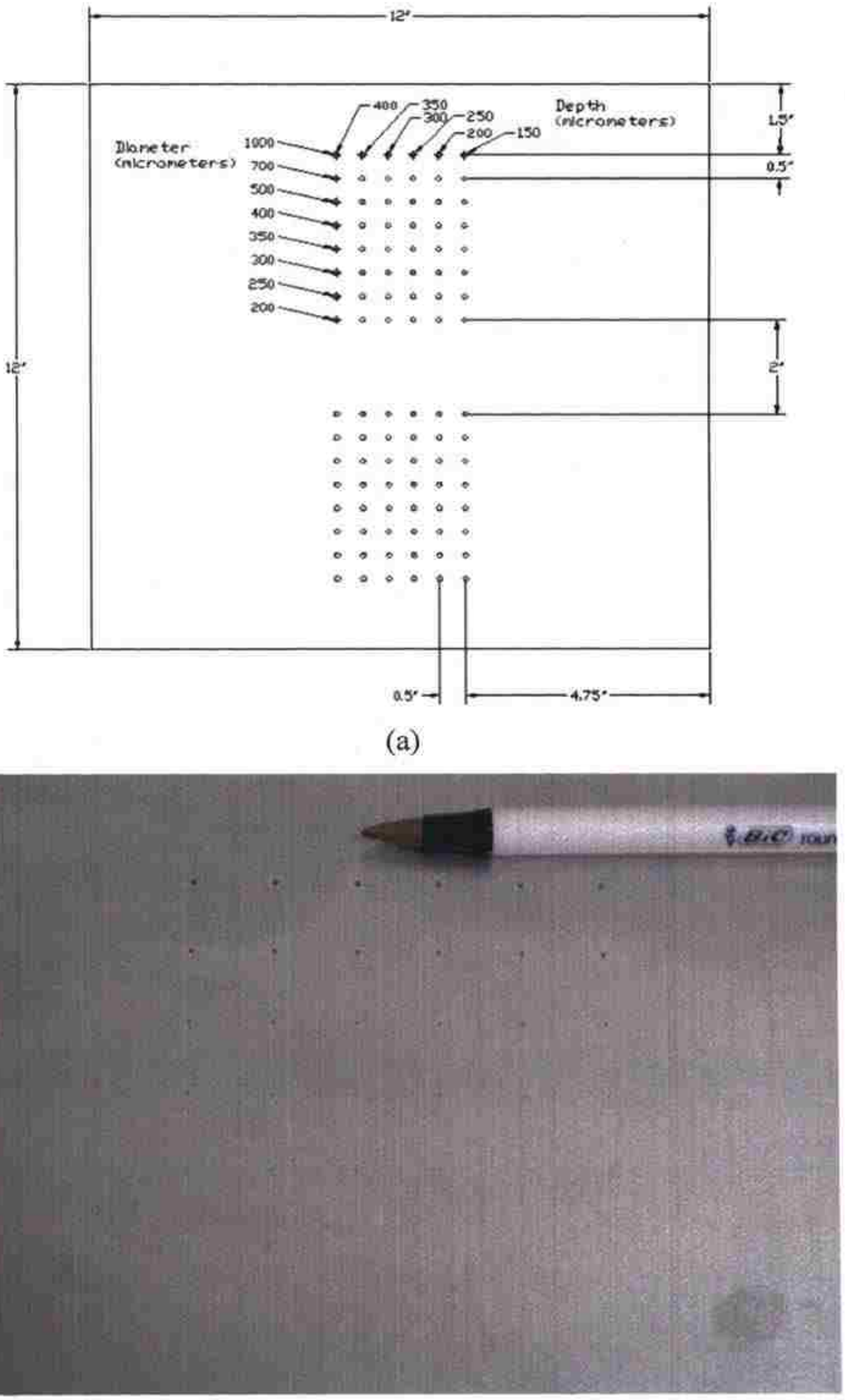

(a)

(b)

Figure 1.4. Laser cut pits sample: a) schematic and b) picture.

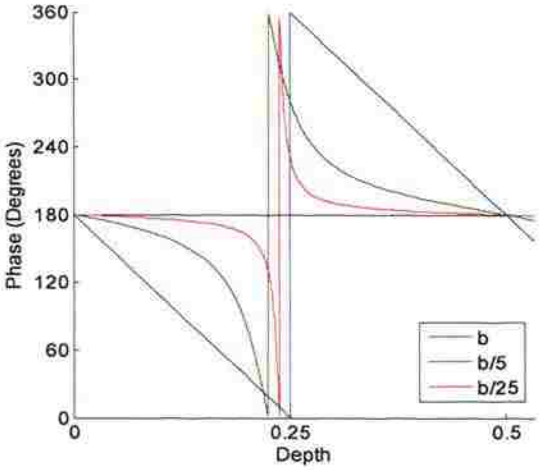

Figure 2.1. Simulated phase of reflection coefficient as a function of electrical depth (depth is given relative to wavelength) for empty cracks in a perfect electric conductor with three widths (including $W = b$, matched waveguide case). Simulations were performed at 10.3 GHz (X-band) with varying physical depth.

Figure 2.2 shows the phase of reflection coefficient as a function of frequency for cracks with several depths and widths at V-band. Figure 2.2a shows the phase of reflection coefficient for cracks with $W = 0.25$ mm and four different depths. The variation of the depth shifts the resonant frequency; in particular, shallower scratches cause the transition to occur at higher frequencies. This shift of resonant frequency occurs as described in (2) and is the foundation of this depth evaluation approach. Figure 2.2b shows the phase of reflection coefficient for cracks with $D = 1.27$ and four different widths, indicating that cracks with smaller widths have a more abrupt or sharper phase transition. These relationships have also been previously observed [18].

It was shown in [35] that the magnitude of reflection coefficient for a quarter-wavelength short-circuited waveguide changes slightly (decreases) if the conductor losses in waveguide walls are taken into account. In this investigation several cracks in metal plates with different conductivities were investigated and it was observed that *narrow* quarter-wavelength short-circuited cracks exhibit resonant behavior in the magnitude of reflection coefficient as well as in the phase. For instance, Figure 2.3 shows the simulated frequency dependence of the complex reflection coefficient, for cracks with $D = 1.03$ mm and five different widths, in an aluminum plate with a conductivity of

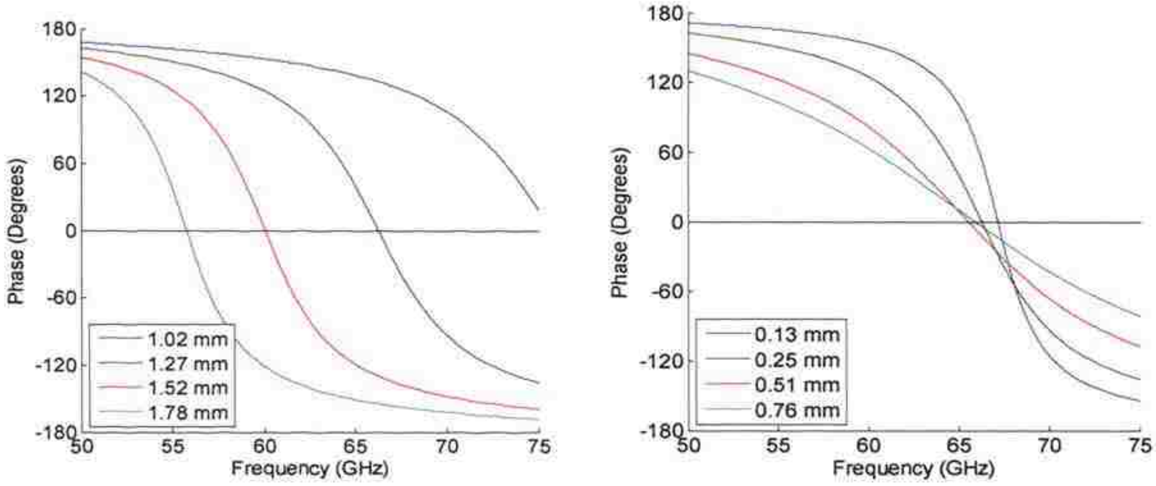

(a) (b)

Figure 2.2. Simulated phase of the reflection coefficient as a function of frequency for empty cracks with several depths and widths at V-band: a) $W = 0.25$ mm and four depths, and b) $D = 1.27$ mm and four widths.

$\sigma = 3.72x10^7$ (S/m) at W-band. The probing waveguide dimensions for this band are a = 2.4 mm and b = 1.3 mm, respectively. As shown in Figure 2.3a, the magnitude of reflection coefficient no longer remains constant (e.g., $|\Gamma| = 1$) and exhibits a resonant response for narrow crack widths. This resonant response has a minimum at the resonant frequency corresponding to the quarter-wavelength resonance. At least two important observations can be made from Figure 2.3a. First, the resonant frequency of the quarter-wavelength short-circuited crack may be found from the magnitude of reflection coefficient, and its depth can then be evaluated using (2). Second, the Q-factor and magnitude at the resonance are highly dependent on crack width and must be considered in determining the measurability of the resonant frequency. In particular, Figure 2.3a shows that $|\Gamma|$ at the resonance is non-monotonically dependent on width. For instance, for the widest cracks (W = 1.3 and 0.2 mm), $|\Gamma|$ is close to 1. However, as the width decreases, $|\Gamma|$ initially decreases and approaches zero (shown by the crack with W = 0.022 mm). As the width is further decreased, $|\Gamma|$ increases (e.g., $|\Gamma|$ = 0.65 for the crack with W = 0.01) and approaches 1 as the width is reduced to zero (not shown in Figure 2.3a). It should be noted that the resonant frequency is relatively insensitive to crack width for the

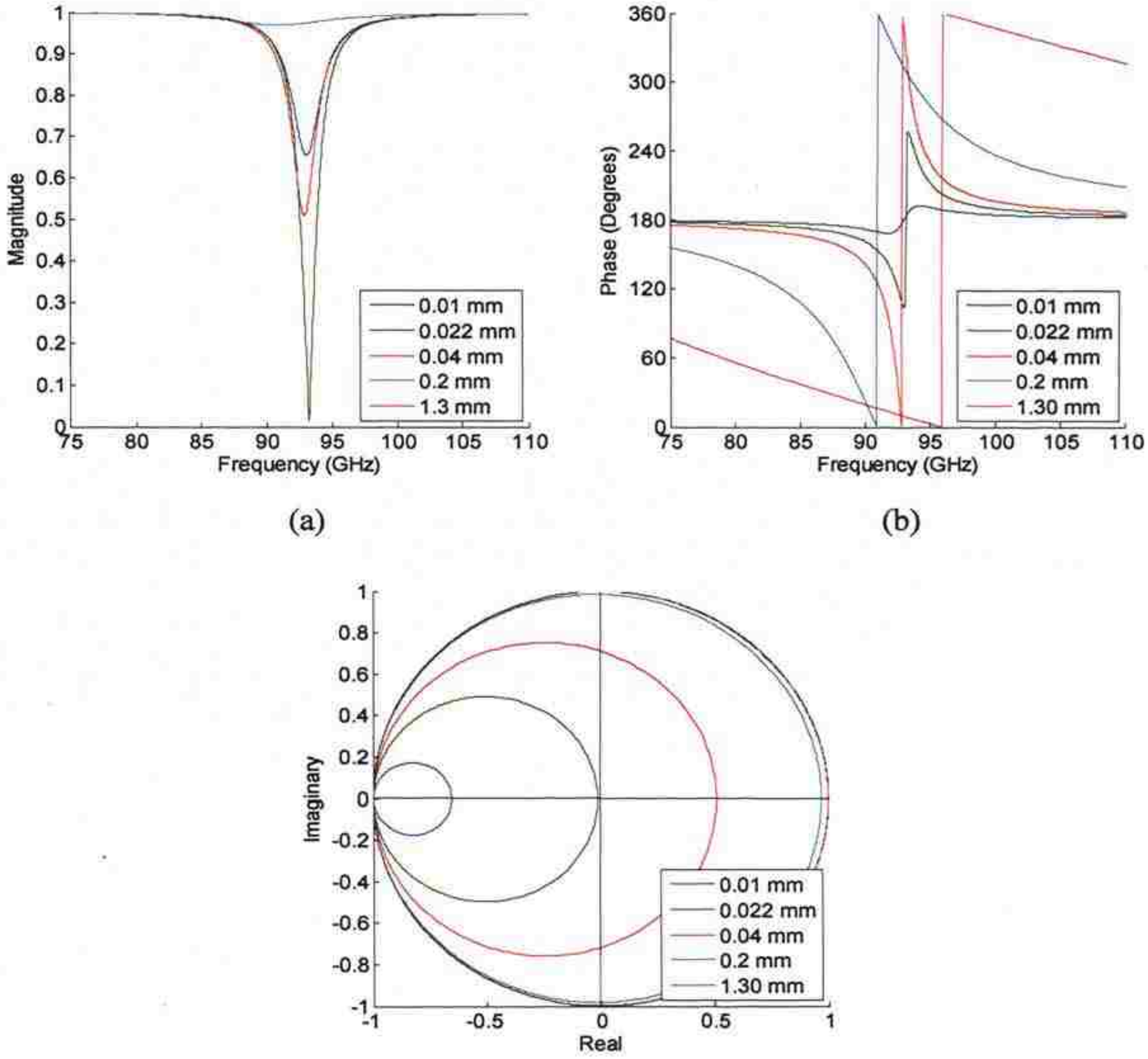

(a)

(b)

(c)

Figure 2.3. Simulated complex reflection coefficient of empty cracks in aluminum with $D = 1.03$ mm and five widths at W-band: a) magnitude and b) phase of the reflection coefficient as a function of frequency, and c) reflection coefficient in the complex polar plane.

range of 0.01–0.04 mm, as shown in Figure 2.3a. This observation is confirmed by the phase of reflection coefficient, shown in Figure 2.3b.

Plotting the results in the complex polar plane provides some additional insight to the resonance behavior, as shown in Figure 2.3c. In this format where the complex

undercoupled region the loaded *Q*-factor is related to the conductor *Q*-factor, as will be shown.

The condition of critical coupling is $Q_e = Q$, so the loaded *Q*-factor at critical coupling can be determined from (3) – (6) and is shown in Figure 2.4b as the dashed curves. A filling factor of 0.55 was used to match this curve to the points of critical coupling, which implies that a large portion of the resonant field extends into the probing waveguide.

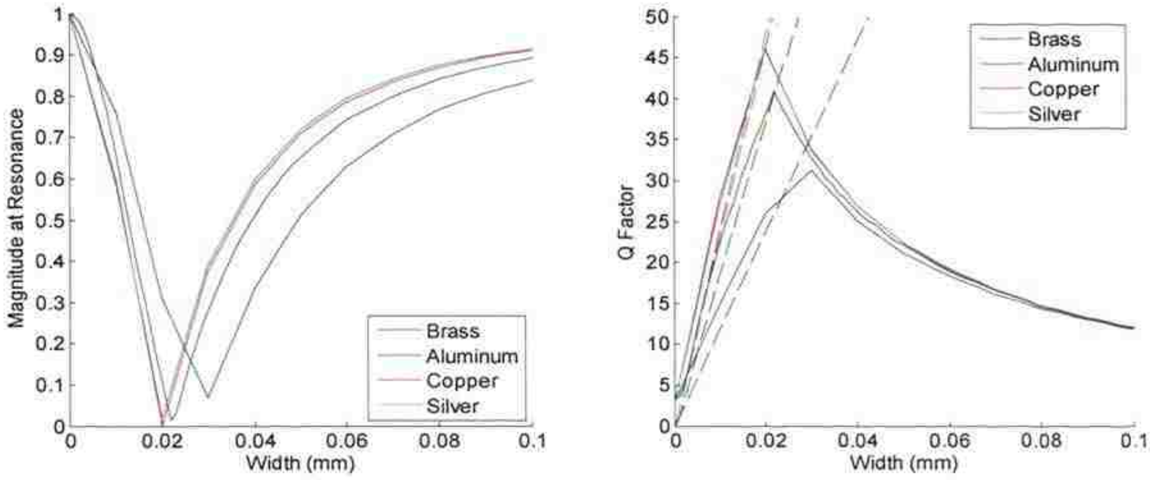

(a) (b)

Figure 2.4. Simulated characteristics of resonant response as functions of width for empty cracks in four metals with $D = 1.03$ mm at W-band: a) magnitude of reflection coefficient at resonant frequency and b) *Q*-factor. In b) the solid lines are from simulation and the dotted lines are $Q_C/2$ from (3) – (6).

The described features of the resonant responses can be explained by the coupling between the probing waveguide and the crack. From (7) it can be seen that at critical coupling ($g = 1$) the resonator is matched to the probing waveguide ($Q_c = Q_e$). If the aluminum conductor case is considered, the results for $W = 0.022$ mm correspond to critical coupling in which $\Gamma = 0$ at the resonant frequency (Figure 2.3a) and the loaded *Q*-factor is also maximum at this width (Figure 2.4b). As the width decreases the conductor loss increases (Eq. (6)) and the resonator becomes undercoupled (g < 1, e.g., *W* = 0.01 mm) resulting in a reduction in the *Q*-factor. When W > 0.022 mm the resonator is overcoupled (g > 1, e.g., W = 0.04 mm), approaching the case when the entire signal is coupled into the crack (e.g., at *W* = 0.2 mm). In this case the external (to the crack) loss becomes dominant, causing the decrease in the loaded *Q*-factor.

2.1.3. Sensitivity Analysis. Using (2) to evaluate crack depth, by measuring the resonant frequency, shows no dependence on crack width since it is a close approximate form for evaluating crack depth (i.e., only considers the crack geometry). However, the simulations which include the entire structure, and are hence more accurate, showed some dependency between crack width and its resonant frequency. Therefore, to determine the sensitivity of evaluating crack depth using (2) to crack width, the following was considered. Simulations were conducted for several combinations of crack widths and depths (i.e., "actual" widths and depths). Subsequently, the resonant frequencies from the simulations (in effect representing actual measurements) were used in conjunction with (2) to estimate the depth. Three depths of *D* = 0.92, 1.1, and 1.41 mm, were used with varying widths in W-band. Figure 2.5 shows the error in depth estimation (compared to the depth used in simulation) as a function of crack width normalized to *b*, for three

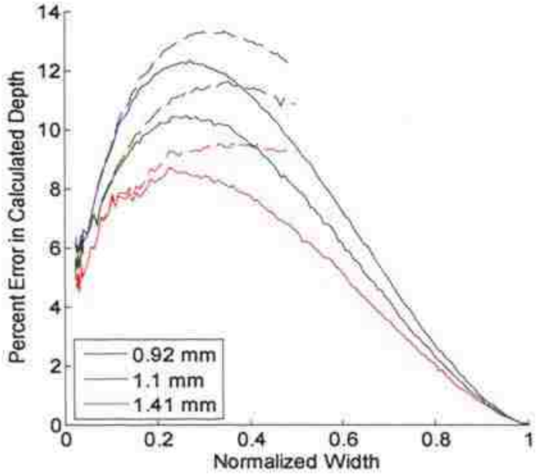

Figure 2.5. Simulated error in depth evaluation as a function of width (normalized to *b*) for empty cracks in aluminum with three depths at W-band: using phase (solid) and magnitude (dashed) of reflection coefficient.

and width, for a crack with $L \geq 1.7a$ this error could be corrected by multiplying the measured resonant frequency by a constant.

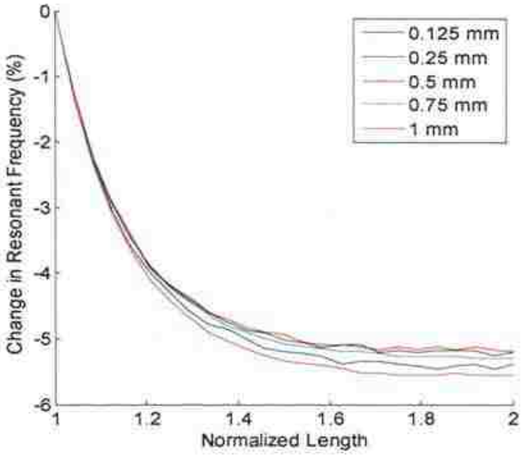

Figure 2.6. Simulated percentage change in resonant frequency as a function of crack length (normalized to a) for empty cracks in aluminum with $D = 1$ mm and five widths at W-band.

2.1.4. Measurement Results. Measurements were performed on cracks with $W = 0.5$ mm and three depths in an aluminum plate at K-band using a VNA. Figure 2.7 shows the measured and simulated frequency dependence of the complex reflection coefficient for cracks with $W = 0.5$ mm and three depths at K-band. Figure 2.7a shows the phase of reflection coefficient with accompanying simulations (the simulations were performed using cracks in a perfect electric conductor). The measurements match the simulation results quite well, with similar curves for each depth and the resonant frequencies differing by less than 3%. The measurement results show the resonant response for all three cracks. The resonant frequency is clearly shifted as a function of crack depth, as expected. Figure 2.7b shows the measured magnitude of reflection coefficient for the same cracks. Dips can be observed in the magnitude for each crack which by comparison to Figure 2.7a, occur at the resonant frequencies. These are the consequence of conductor losses, as described previously, and are small since these cracks are much wider than the width for critical coupling. Figure 2.7c shows these measurements in the complex plane.

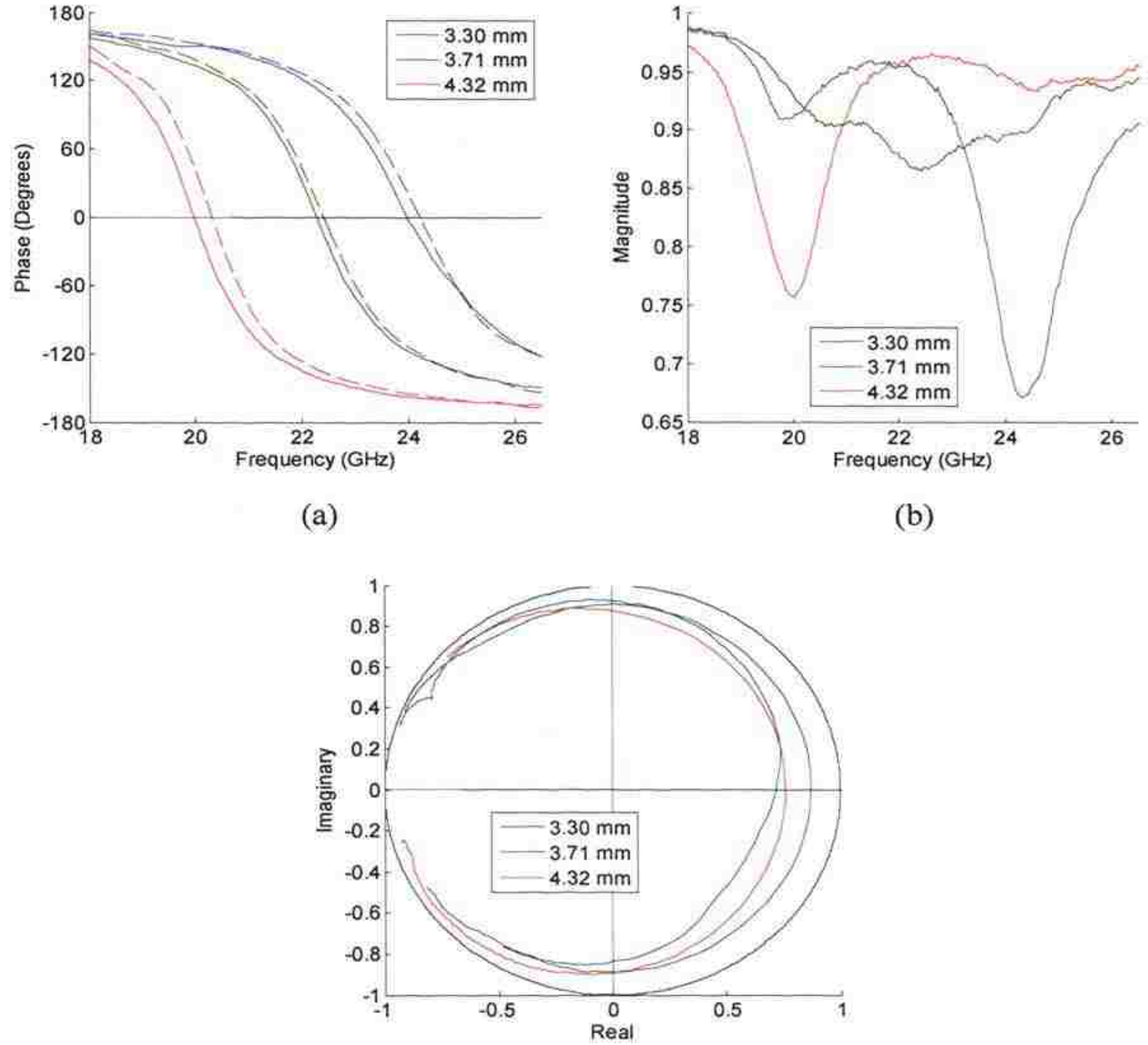

(a)

(b)

(c)

Figure 2.7. Measured (solid) and simulated (dashed) complex reflection coefficient of empty cracks in aluminum with $W = 0.5$ mm and three depths at W-band: a) magnitude and b) phase of the reflection coefficient as a function of frequency, and c) reflection coefficient in the complex polar plane.

The resonant circles are clearly seen and have a radius close to one, indicating that the cracks are highly overcoupled.

Figure 2.8 shows a comparison of the estimated depth using the described method and the actual crack depth (measured by a micrometer), for the K-band measurements shown in Figure 2.7. The resonant frequencies were found from the zero in the phase of reflection coefficient, and the depth was estimated using (2). Figure 2.8a clearly shows the ability of this method to estimate crack depth. However, error in depth estimation may be as much as 20%. Figure 2.8b shows the estimated depth with the correction factor (from (9)) for width, which reduced the error to 12%. Sources of this error may include the positioning of the waveguide over the crack, the approximation of the crack length to equal the waveguide *a* dimension used in the derivation of (2), and error in the measurement of "actual" crack depth.

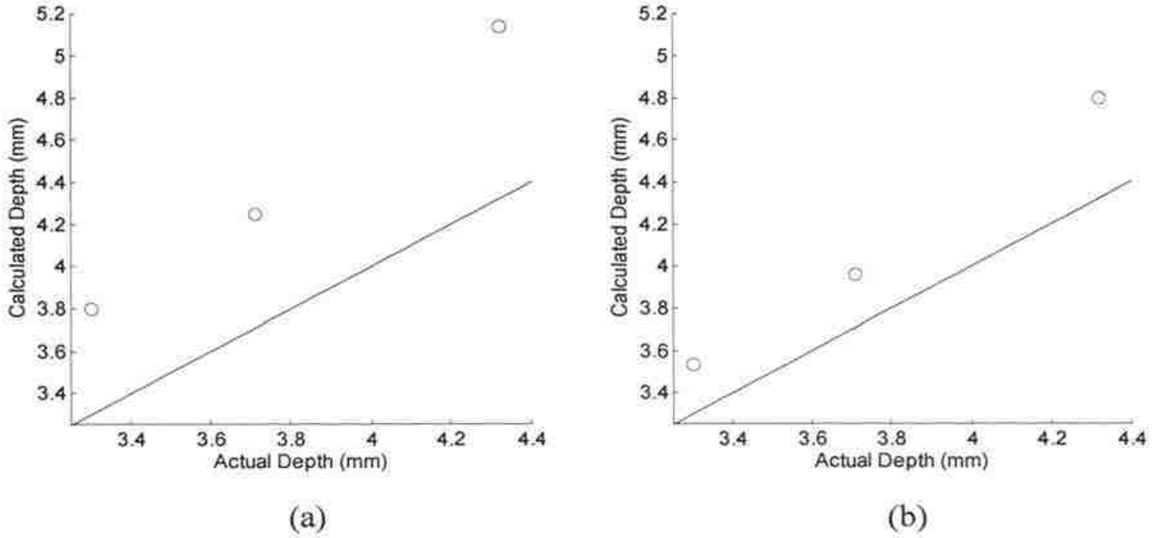

(a) (b)

Figure 2.8. Comparison of depth calculated from measurements (using Equation (2)) to actual depth (as measured by micrometer) for K-band measurements: a) without and b) with correction factor for width.

2.1.5. Cracks Shallower than a Quarter-Wavelength. It may not be possible to provide very high frequency measurements to observe the quarter-wavelength resonance for very shallow damage. It may also be desirable for ease of measurement or design of measurement systems to use single frequency measurements. Consequently, the use of the phase of reflection coefficient to evaluate depth was investigated for cracks shallower than a quarter-wavelength.

Figure 2.9 shows the measured (solid) and simulated (dashed) phase of reflection coefficient for cracks with two widths and several depths at W-band. For each of the cracks in Figure 2.9 the depth is less than a quarter-wavelength and, consequently, the resonant frequency will be higher than the operating frequency band. The measured data show some variance from the simulations, with in general a greater phase change in measurement than simulation. However, for each width, in both simulation and measurement, the curves are sorted by depth with deeper cracks resulting in a larger phase change. This is expected since the resonant frequency will be lower, and thus closer to the operating frequency band, for the deeper cracks than for the shallower cracks. Since the resonant frequency is closer more of the tail of the resonant response is seen. The cracks in Figure 2.9a have a diameter of 0.51 mm while the cracks in Figure 2.9b have a diameter of 1.02 mm. The wider cracks in Figure 2.9b result in a larger phase change than in Figure 2.9a, which is also expected since wider cracks have a more gradual phase change in the resonant behavior (Figure 2.2b), the effects of which will extend further in frequency. If two curves of different width but a common absolute phase of ~150° at 75 GHz, e.g. 0.46 mm in Figure 2.9a and 0.29 mm in Figure 2.9b, are

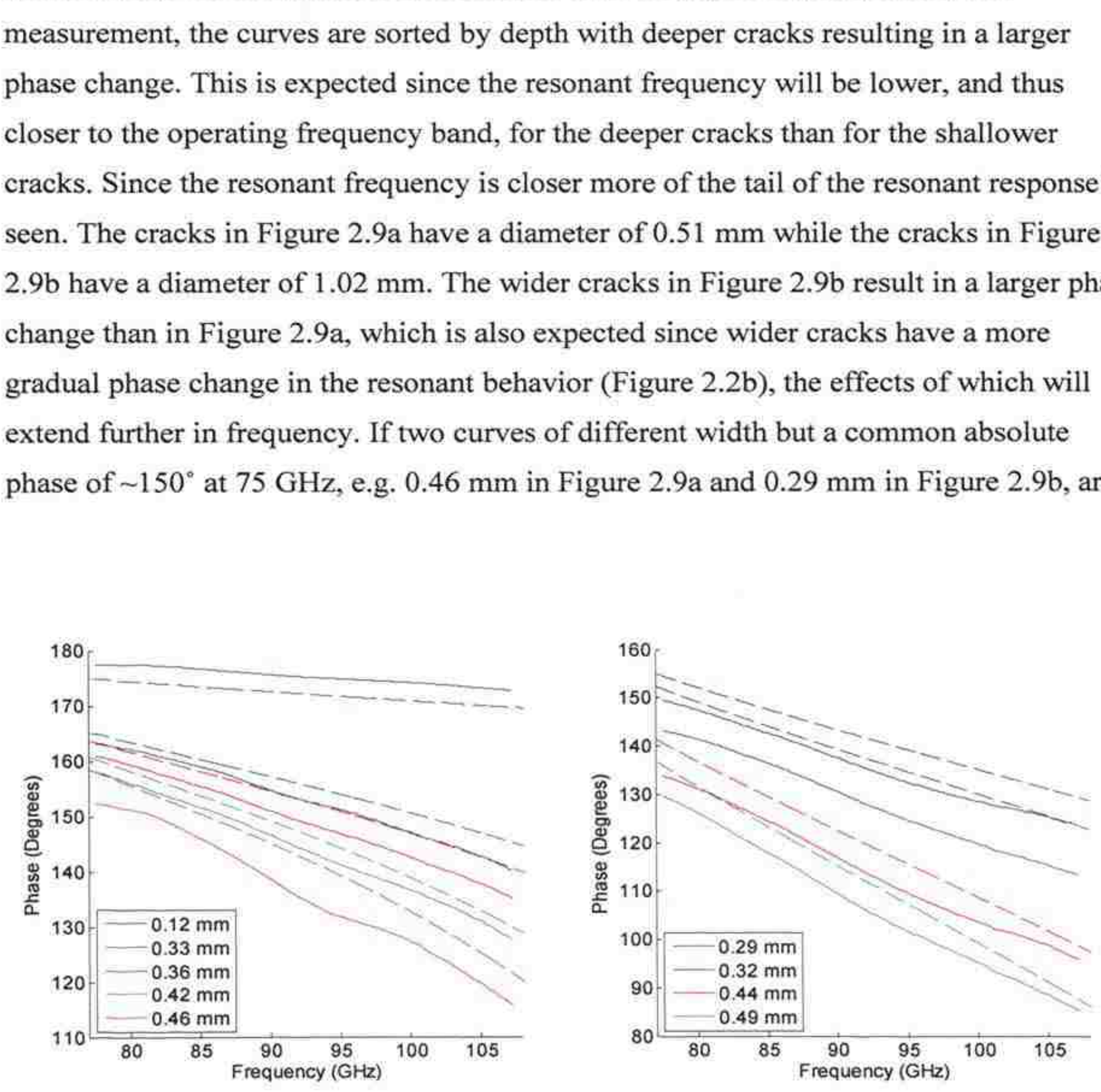

(a) (b)

Figure 2.9. Measured (solid) and simulated (dashed) phase of reflection coefficient as a function of frequency for empty cracks in aluminum with two widths and several depths at W-band: a) $W = 0.51$ mm with five depths and b) $W = 1.02$ mm with four depths.

compared it can be observed that the slopes are different. So it should be possible to distinguish between the effects of depth and width if the phase is known for at least two frequency points, and crack depth could then be evaluated.

2.2. FINITE CRACKS

Finite cracks present a more complex electromagnetic problem than long cracks, since several additional boundaries are introduced and the length of the crack becomes important as an additional geometrical parameter. The behavior can be somewhat similar to long cracks, however, if the crack length is sufficient to support a propagating mode for a portion of the frequencies within the band. Equation (2) is a valid approximation as long as a propagating mode is supported; otherwise the quarter-wavelength resonance cannot exist.

Simulations were performed to determine the frequencies that can be propagated for various crack lengths, as shown in Figure 2.10. Figure 2.10a shows the simulation geometry. The signal coupled from port 1 to port 2 will be very small if no propagating mode is supported in the crack since in that case the signal will be significantly

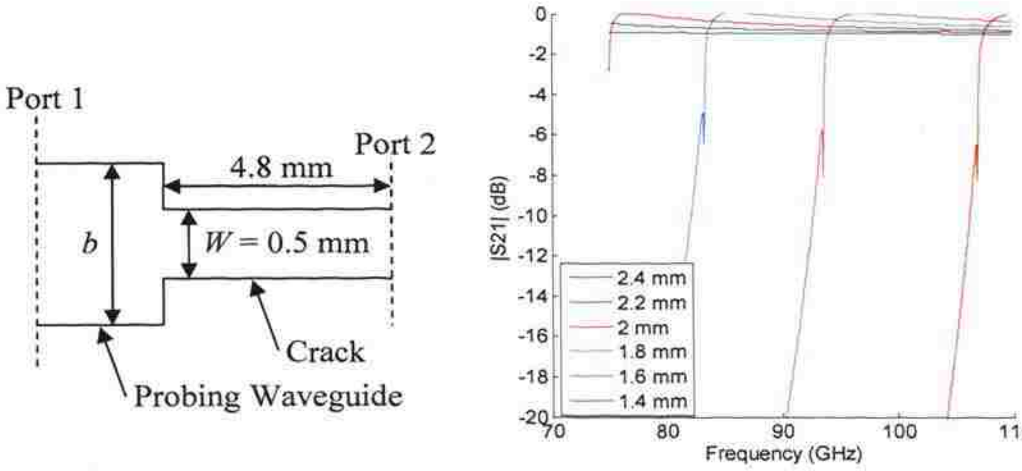

(a) (b)

Figure 2.10. Simulated signal transfer from a probing waveguide to an empty finite crack at W-band: a) side-view of simulation schematic (not-to-scale) and b) $|S_{21}|$ for 6 crack lengths.

attenuated as it travels the 4.8 mm in the crack to port 2. Figure 2.10b shows $|S_{21}|$ for cracks in a perfect electric conductor with 6 different lengths at W-band. It is observed that $|S_{21}|$ is reasonably high for the 2.4 and 2.2 mm long cracks over the entire frequency band, so these cracks will support a propagating mode for the full band. The 2, 1.8, 1.6, and 1.4 mm long cracks each have a sharp drop in $|S_{21}|$, where for lower frequencies a propagating mode is not supported and for higher frequencies one is supported. Following the trend of this figure, and according to well-known waveguide equations, for cracks with $L \leq 1.2$ mm = $a/2$ no propagating mode will be supported within the frequency band.

Figure 2.11 shows the simulated phase of reflection coefficient for cracks with D = 1.4 mm, W = 0.5 mm, and ten different lengths, starting from $L = a = 2.4$ mm, at W-band. It is seen that the frequency where the phase crosses zero (the resonant frequency) shifts to the right (higher frequencies) as the crack length decreases, as would be expected from (2). Furthermore, this shift accelerates as the length is reduced. For sufficiently long cracks where a propagating mode is supported for some portion of the frequency band, with a proper depth, a resonance may be observed, as shown in Figure 2.11a. If the length is further reduced the resonance first shifts out of the frequency band

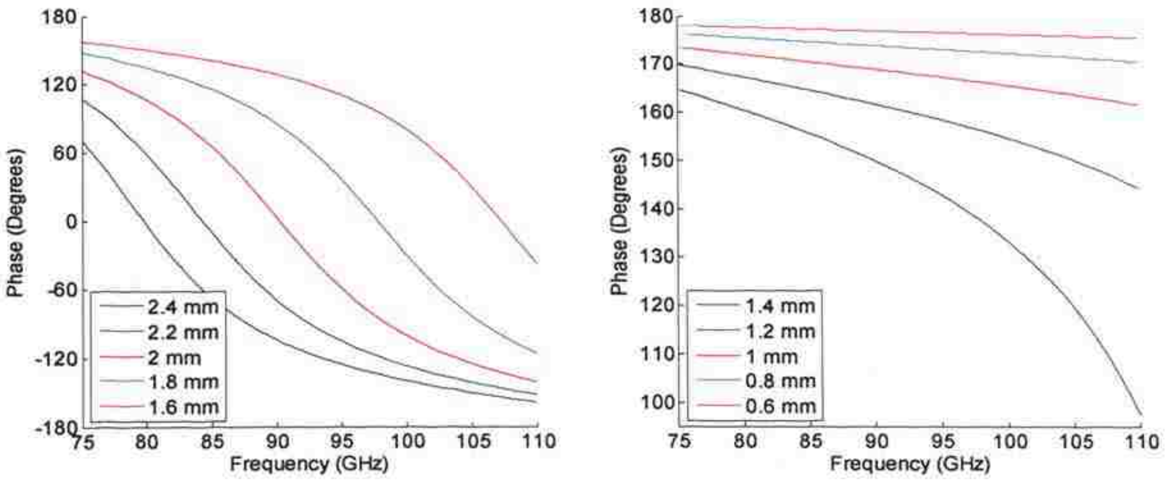

(a) (b)

Figure 2.11. Simulated phase of reflection coefficient as a function of frequency for empty cracks in aluminum with D = 1.4 mm, W = 0.5 mm, and ten lengths at W-band.

(e.g., 1.4 mm crack in Figure 2.11b), and at some shorter length the crack will cease to support propagating modes for the entire frequency band (1.2–0.6 mm cracks in Figure 2.11b). For cracks where the resonant frequency can be evaluated it is possible to use the quarter-wavelength resonance and (2) to estimate depth (as will be shown). For shorter cracks the phase change which is still observed may contain some information about the crack depth.

Figure 2.12 shows the percent error in depth estimation using (2) and the simulations shown in Figure 2.11a. It is seen that the error is relatively small, and in fact offsets some of the error from the previously-described width dependency. This is reasonable since when the crack length is reduced current can flow around the edges of the crack, which would tend to have an inductive effect. The capacitive effect of the crack width, as described previously, would then be partially cancelled by this inductive effect. It is important to note that this method can only be applied to cracks with a known length which is greater than *a*/2.

Figure 2.13 shows the simulated phase of reflection coefficient as a function of crack depth for cracks with $W = 0.5$ and 4 lengths which will not support a propagating mode at 92.5 GHz (W-band). For each length the phase converges to a minimum value, and the depth beyond that point cannot be seen. This is due to the limited penetration of

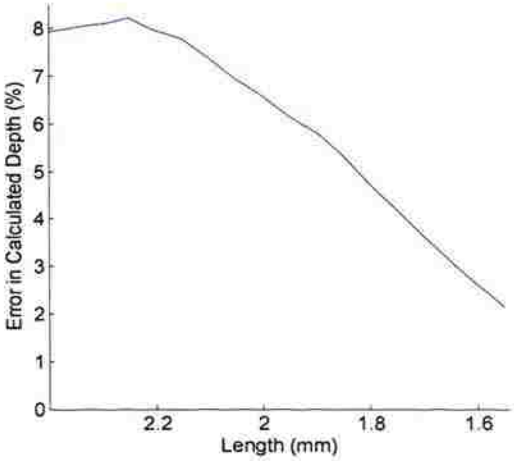

Figure 2.12. Percent error in depth calculated from the measurements shown in Figure 2.11a using (2) compared to the actual simulation depth.

evanescent modes. It is also observed that shorter cracks converge for smaller depths and to a lesser phase change than longer cracks, e.g., the phase of the 0.6 mm long crack levels off around a depth of 0.4 mm, while the phase of the 1.2 mm long crack is continuing to change at a depth of 1 mm. Consequently, if the crack length is known (the width will likely be needed as well, as shown in Figures 2.9a-b for long cracks) the phase can be used to find the depth if the crack is sufficiently shallow or, if the crack is not sufficiently shallow, to know that the crack width is greater than some depth which is the maximum penetration of the signal.

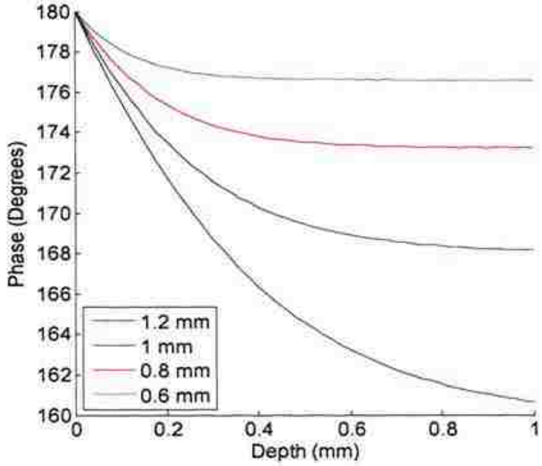

Figure 2.13. Simulated phase of reflection coefficient as a function of crack depth for empty cracks in aluminum with $W = 0.5$ and 4 lengths at 92.5 GHz (W-band).

The sensitivity to position, within the probing waveguide aperture, is an important consideration for finite cracks. The crack position may be varied in two dimensions and it may also be more difficult to accurately position the probing waveguide over the crack, since for finite cracks no portion of the crack extends outside the waveguide aperture. A rectangular crack with $L = a/2 = 1.2$ mm, $W = 0.5$ mm, and $D = 1$ mm was simulated with the crack center at various locations in the waveguide aperture at W-band. The setup and results are shown in Figure 2.14. The position was varied along three directions as shown in Figure 2.14a. Only one quadrant was considered since the waveguide is symmetric in both directions. Figure 2.14b shows the phase at 92.5 GHz as a function of the normalized offset for each of the three paths. The shift along path *a* has a significant and immediate effect upon the measured phase, indicating that this measurement is strongly dependent on variations along this direction. The change in phase is more gradual and much smaller along path *b* so the position along this dimension is not critical, which is expected since the electric field in the probing waveguide is uniform in this direction. A greater effect is observed as the crack nears the edge of the waveguide. The change in phase along path *c* is very close to that along path *a*, indicating that in the presence of shifts in both dimensions the shift along *b* has no discernable effect and only the shift along *a* is significant.

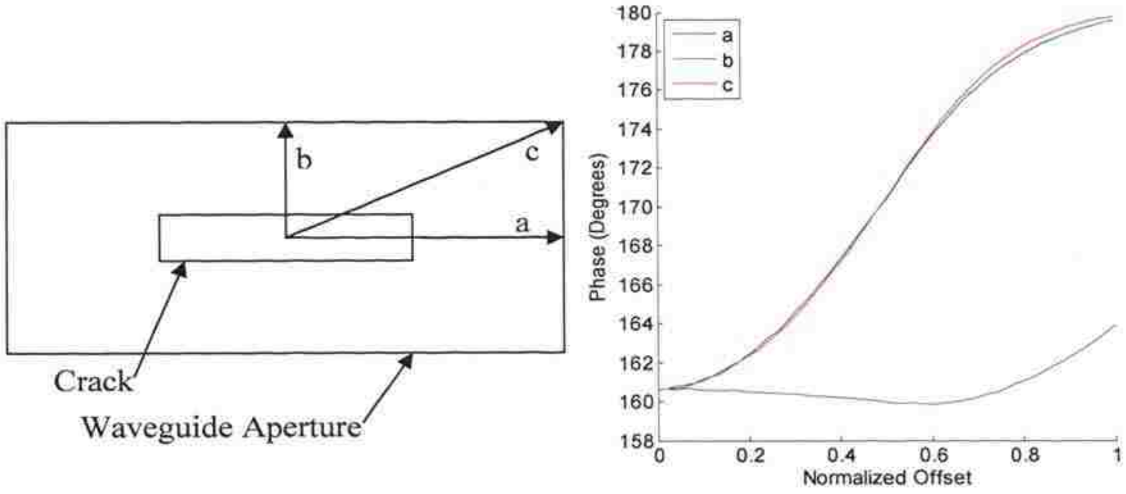

(a) (b)

Figure 2.14. Simulated empty finite cracks in aluminum with $D = 1$ mm, $W = 0.5$ mm, and $L = a/2 = 1.2$ mm at 92.5 GHz (W-band): a) Plan-view of finite crack in waveguide aperture and three paths of shifting crack position (not-to-scale), and b) simulated phase of the reflection coefficient along each path as a function of position along the path (each path is normalized to its length).

2.3. PITS

Pits with openings that can be contained within the waveguide aperture will have diameters much less than *a* and, thus, will not support propagating waves. Consequently, the quarter-wavelength resonance phenomenon cannot be used. However, the presence of a pit changes the reflection coefficient and information about the damage depth may be extracted from this change.

Figure 2.15 shows the phase of reflection coefficient as a function of frequency for pits with diameter of 1.0 mm and four different depths. The simulation results in Figure 2.15a not only show the presence of a pit (i.e., phase different than 180°), but also that the phase is a function of pit depth. Figure 2.15b shows measurement results of pits with similar dimensions. It can be seen that the behavior of the pits with respect to depth is similar for simulation and measurement. There is an absolute shift of a few degrees between measurement and simulation, but this is likely from error in the measurement calibration. The measured results for the 0.33 mm-deep pit show a localized dip in phase around 100 GHz, but this is not seen in simulation or the other measurements and is likely measurement error due to the probe position shifting during the measurement.

Figure 2.16 shows measurement results of pits at a different frequency band or with a different diameter than those shown in Figure 2.15. Figure 2.16a shows measurement results of the same pits as shown in Figure 2.15b, but at V-band. The phase

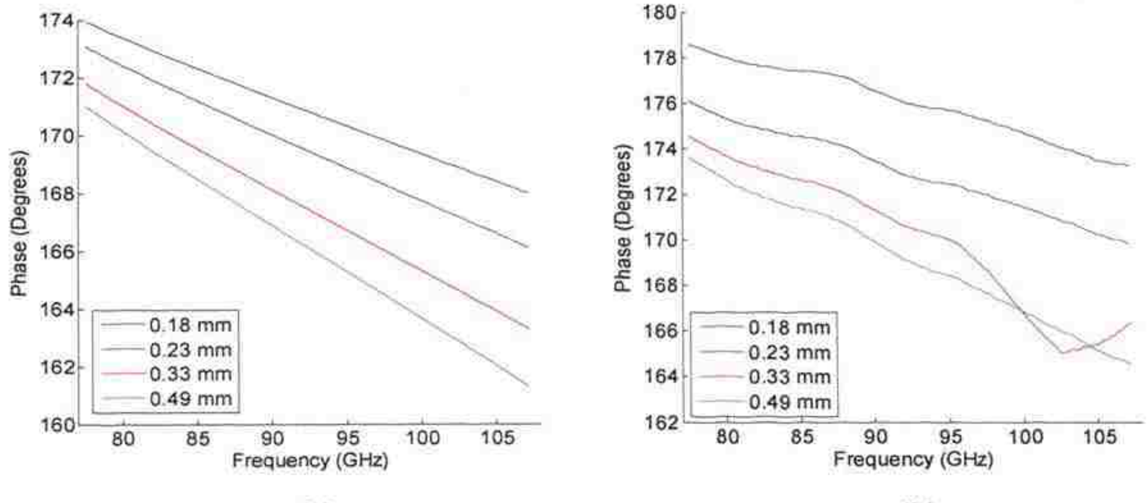

(a) (b)

Figure 2.15. Simulated and measured phase of reflection coefficient as a function of frequency for pits in aluminum with a diameter of 1.0 mm and four depths at W-band: a) simulated and b) measured.

change is much smaller at V-band, as expected since at lower frequencies the pits are electromagnetically smaller in both depth and diameter. However, the curves are still ordered by depth, with greater phase change caused by the pits with larger depths. The one exception is the 0.49 mm-curve for the lower half of the frequency band. The difference between the measured phase for this crack and that expected from comparison with the other curves is consistent with a change in the phase of reflection coefficient associated with the probing waveguide not being exactly flat on the aluminum plate (i.e. tilted), which was observed in several measurements (not shown). Figure 2.16b shows measurement results of pits with a diameter of 0.7 mm and five different depths at W-band. As expected for the smaller pit diameter, the phase change is also smaller than for the 1 mm-diameter pit results shown in Figure 2.15b. The curves are not sorted by depth in this case, which suggests that for this small of pits measurement error from sources such as probe position may be more significant than the influence of depth.

Figure 2.17 shows the simulated phase of reflection coefficient as a function of pit depth for pits in an aluminum plate with six different diameters at 92.5 GHz. For each

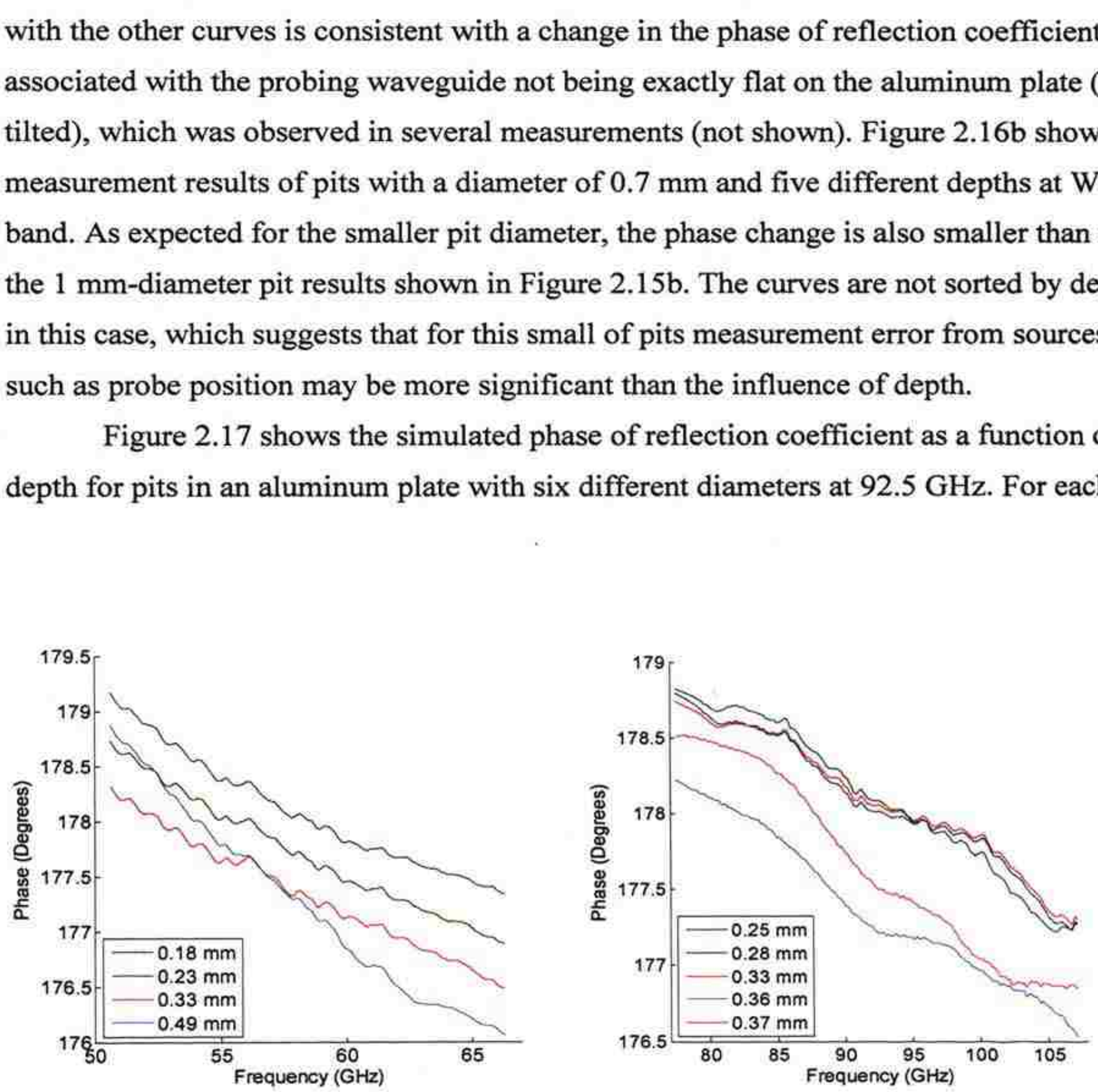

(a) (b)

Figure 2.16. Measured phase of reflection coefficient as a function of frequency for empty pits in aluminum with two diameters and several depths at V-band and W-band: a) pits with diameter of 1.0 mm and four depths at V-band and b) pits with diameter of 0.7 mm and five depths at W-band.

diameter the phase quickly converges to a minimum value, and the depth beyond that point cannot be seen (as mentioned before, pits with openings significantly smaller than the waveguide cannot support propagating waves and thus penetration is limited for deeper pits as in the case of finite cracks [16]). It is also observed that smaller diameter pits have less effect on the phase. The 0.125 mm-diameter pit has no effect on the phase and cannot even be detected. The 0.75 mm-diameter pit has a maximum of 5° phase shift and for depths less than 0.5 mm the phase can be directly related to pit depth.

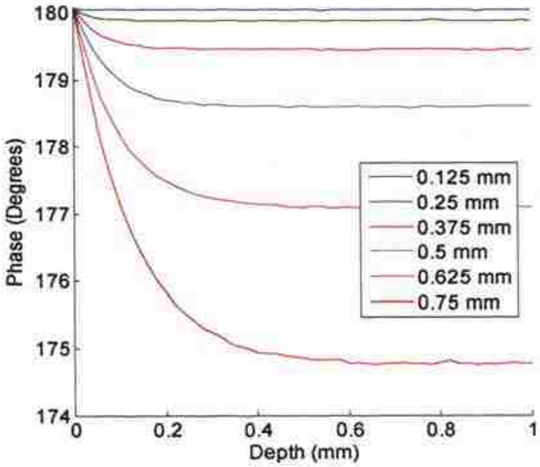

Figure 2.17. Simulated phase of reflection coefficient as a function of depth at 92.5 GHz (W-band) for empty pits in aluminum with six diameters.

3. DIELECTRIC-FILLED DAMAGE

3.1. LONG CRACKS

3.1.1. Approach/Theoretical Background. If a crack is filled with a dielectric material having a relative (to free-space) complex dielectric constant, $\varepsilon_r = \varepsilon_r' - j\varepsilon_r''$ (the real part indicates relative permittivity and the imaginary part indicates relative loss factor), there are two primary differences with respect to an empty crack. First, the crack geometry changes electromagnetically; in particular from (2) it is evident that the guide wavelength in a crack filled with a material with a relative permittivity, $\varepsilon'_r > 1$, is reduced, which makes a shallow crack appear electrically deeper. Consequently, the depth of a crack can be evaluated at a lower resonant frequency in a filled-crack than when it is empty. The electrical crack length and width may be increased as well. Second, losses associated with the dielectric material are introduced to the system, and these are in addition to the conductor losses described previously. The dielectric losses are expected to be more significant than the conductor losses for typical dielectric materials and crack dimensions. For a filled-crack, then, the unloaded *Q*-factor is related to both conductor and dielectric losses and (4) must be replaced with [34]:

$$\frac{1}{Q} = \frac{1}{Q_c} + \frac{1}{Q_d}, \tag{10}$$

where Q_d is the *Q*-factor due to dielectric loss associated with the material filling the crack and can be estimated as [38]:

$$Q_d = \frac{1}{\rho_d \tan\delta} \tag{11}$$

where

$$\tan\delta = {}^{\varepsilon_r''}\!\big/_{\varepsilon_r'} \tag{12}$$

is the loss tangent of the filling material and ρ_d is the electric field filling-factor for the crack (ratio of the electric field energy stored in the dielectric to the electric field energy stored in entire resonant volume). The filling-factor accounts for the portion of the resonant field (in the filled-crack) which may extend into the probing waveguide. Equation (11) is applicable to any waveguide or transmission line filled with a homogeneous dielectric material [34], which is a useful feature for crack depth evaluation since crack shape may not be perfectly rectangular.

3.1.2. Simulation Results. Simulations of dielectric-filled cracks in an aluminum plate were performed for several dielectric materials. Figure 3.1 shows the frequency dependence of the complex reflection coefficient for a crack with $D = 0.25$ mm and $W = 0.25$ mm filled with five dielectric materials, each with $\varepsilon_r' = 10$ but different loss tangents, at W-band. The specific loss tangents were chosen to include under, over and critical coupling, and the lossless dielectric case ($\tan\delta = 0$) as a reference. Figure 3.1a shows, as expected, a resonance behavior in the magnitude of reflection coefficient. It is important to note that the resonant frequency remains constant for all loss tangents, which is expected since the loss tangent does not appear in (2). The results also show that the resonance response minima changes non-monotonically as a function of loss tangent. For instance, if there are only conductor losses in the crack (i.e., $\tan\delta = 0$), the resonance response is barely detected in Figure 3.1a. On the other hand, when dielectric loss is introduced in the crack, $|\Gamma|$ initially decreases, approaching zero at $\tan\delta = 0.06$, and then increases, slowly approaching 1. It should also be noted that there is a slight asymmetry associated with the responses as a function of frequency. This is due to the increased signal attenuation at higher frequencies as the crack becomes electrically deeper. The phase of reflection coefficient, shown in Figure 3.1b, also changes as a function of loss tangent. For $\tan\delta = 0.02$ the phase is very close to the lossless case with a 360° phase transition, for $\tan\delta = 0.06$ it has a more gradual transition except for a very sharp 180° jump at the resonance, for $\tan\delta = 0.18$ it has some variation in phase but does not have the 360° phase transition, and by $\tan\delta = 0.5$ the phase variation has mostly disappeared.

Consideration of the complex reflection coefficients in polar format, as shown in Figure 3.1c, along with the influence of dielectric loss on the coefficient of coupling (as in (7)) allows for a more comprehensive understanding of the resonant behavior of the dielectric-filled crack. The results for tan $\delta = 0.06$, shown in Figure 3.1c, correspond to (near) critical coupling, where there is no reflection from the crack at the resonant frequency. As tan δ increases from 0.06 the resonator becomes undercoupled (g < 1) and the resonant response shrinks towards Γ' = -1, approaching the case of reflection from a metal plate since the signal does not penetrate inside high-loss dielectrics. On the other

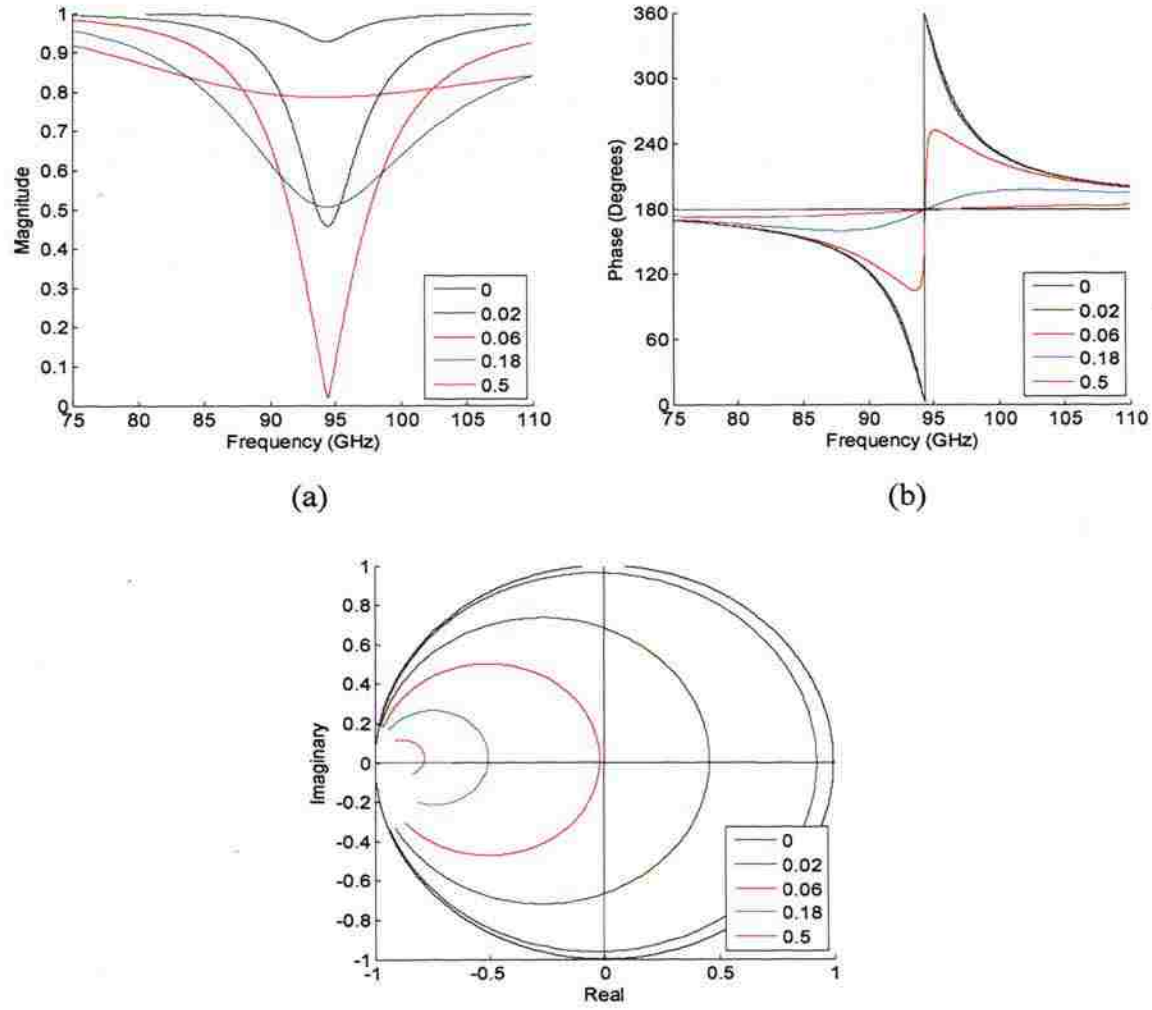

(a)

(b)

(c)

Figure 3.1. Simulated complex reflection coefficient of dielectric-filled cracks in aluminum with $W = 0.25$ mm, $D = 0.25$ mm, $\varepsilon_r' = 10$, and five loss tangents at W-band: a) magnitude and b) phase of the reflection coefficient as a function of frequency, and c) reflection coefficient in the complex polar plane.

hand, when the tan δ decreases beyond 0.06 the resonator is overcoupled ($g > 1$) and the resonant response approaches the case where only conductor loss is considered (i.e., $\Gamma' \sim 1$).

Figure 3.2 shows characteristics of the resonant response as functions of loss tangent for cracks with $D = 0.25$ mm and six different widths. In Figure 3.2a the curve for $W = 0.25$ mm, for example, demonstrates the magnitude of reflection coefficient shown in Figure 3.1a for the full range of considered loss tangents (0 – 0.5) at the resonant frequency (i.e. the magnitude minimum). Figure 3.2a shows that dielectric-filled cracks exhibit resonant behavior for a wide range of widths, from small ($W = 0.06$ mm) all the way to $W = b = 1.3$ mm, with the use of a proper loss tangent (e.g., at tan $\delta = 0.06$ the resonance will be evident for all these widths). Increasing crack width shifts the loss tangent at which critical coupling (magnitude of zero) occurs, and this shift is approximately linear.

Figure 3.2b shows the loaded Q-factor as a function of loss tangent. For each of these curves, as the loss tangent increases the Q-factor smoothly decreases, with a distinct

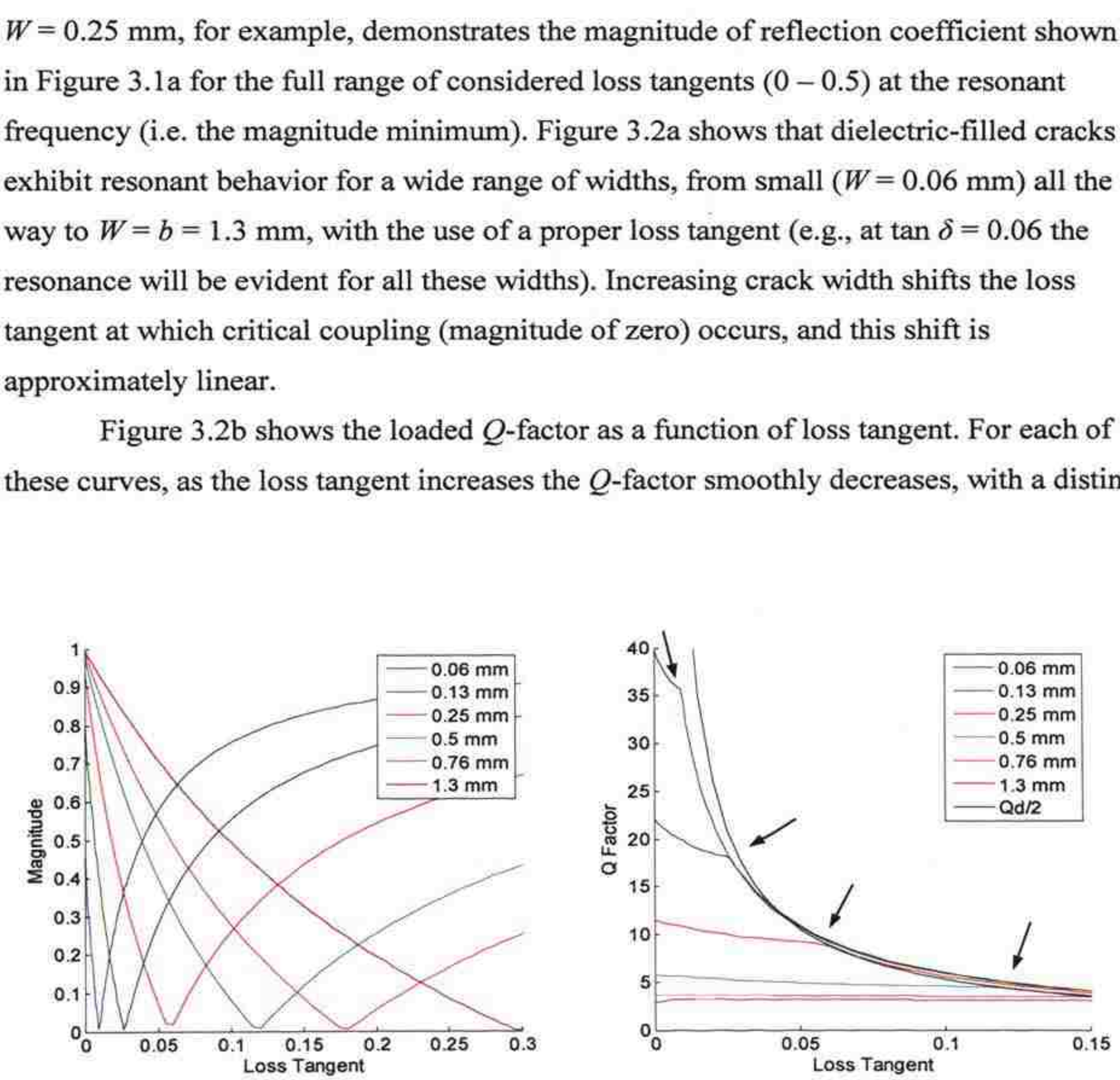

(a) (b)

Figure 3.2. Simulated characteristics of resonant response as functions of loss tangent for dielectric-filled cracks in aluminum with $D = 0.25$ mm, $\varepsilon_r' = 10$, and six widths at W-band: a) magnitude of reflection coefficient at resonant frequency and b) loaded Q-factor. In b) the points of critical coupling are indicated by arrows and the curve $Q_d/2$ from (13) is included.

cracks lengths greater than a. Crack lengths smaller than the broad waveguide dimension will be considered as finite cracks in a separate section.

Using (2) to evaluate crack depth, by measuring the resonant frequency, shows no dependence on crack width since it is a close approximate form for evaluating crack depth (i.e., only considers the crack geometry). However, as for empty cracks, the simulations which include the entire structure, and are hence more accurate, showed some dependency between crack width and its resonant frequency. Therefore, to determine the sensitivity of evaluating crack depth using (2) to crack width, the following was considered. Simulations were conducted for several combinations of crack widths and depths (i.e., "actual" widths and depths). Subsequently, the resonant frequencies from the simulations (in effect representing actual measurements) were used in conjunction with (2) to estimate the depth. Three depths of $D = 0.23$, 0.26, and 0.31 mm, were used with varying widths at W-band. Figure 3.3 shows the error in depth estimation (compared to the depth used in the simulation) as a function of crack width normalized to b, for three depths using the phase (solid) and magnitude (dashed) of reflection coefficient to find the resonant frequency. The results using the phase show that there is less than 3.5% error in

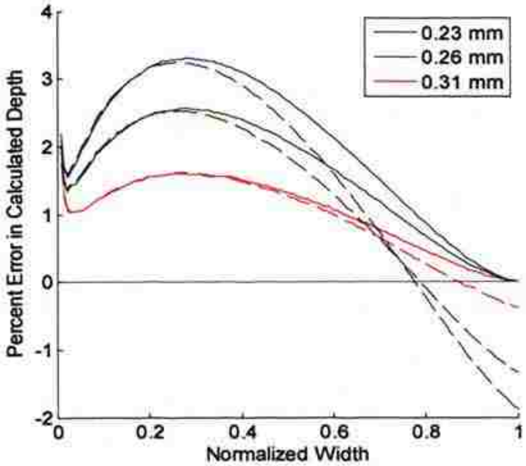

Figure 3.3. Percent error in depth estimation as a function of crack width using phase (solid) and magnitude (dashed) of reflection coefficient for simulated cracks in aluminum filled with a dielectric ($\varepsilon_r' = 10$, $\tan\delta = 0.06$) and with three depths at W-band. Widths are normalized to the probing waveguide b dimension.

was set equal to *a*. Consequently, if the position of the damage, while still extending outside of the probing waveguide aperture, is shifted along its length there is no change to the crack in the simulation. However, the influence of positioning of the crack along *b* needs to be investigated. Figure 3.4c shows the change in the resonant frequency as a

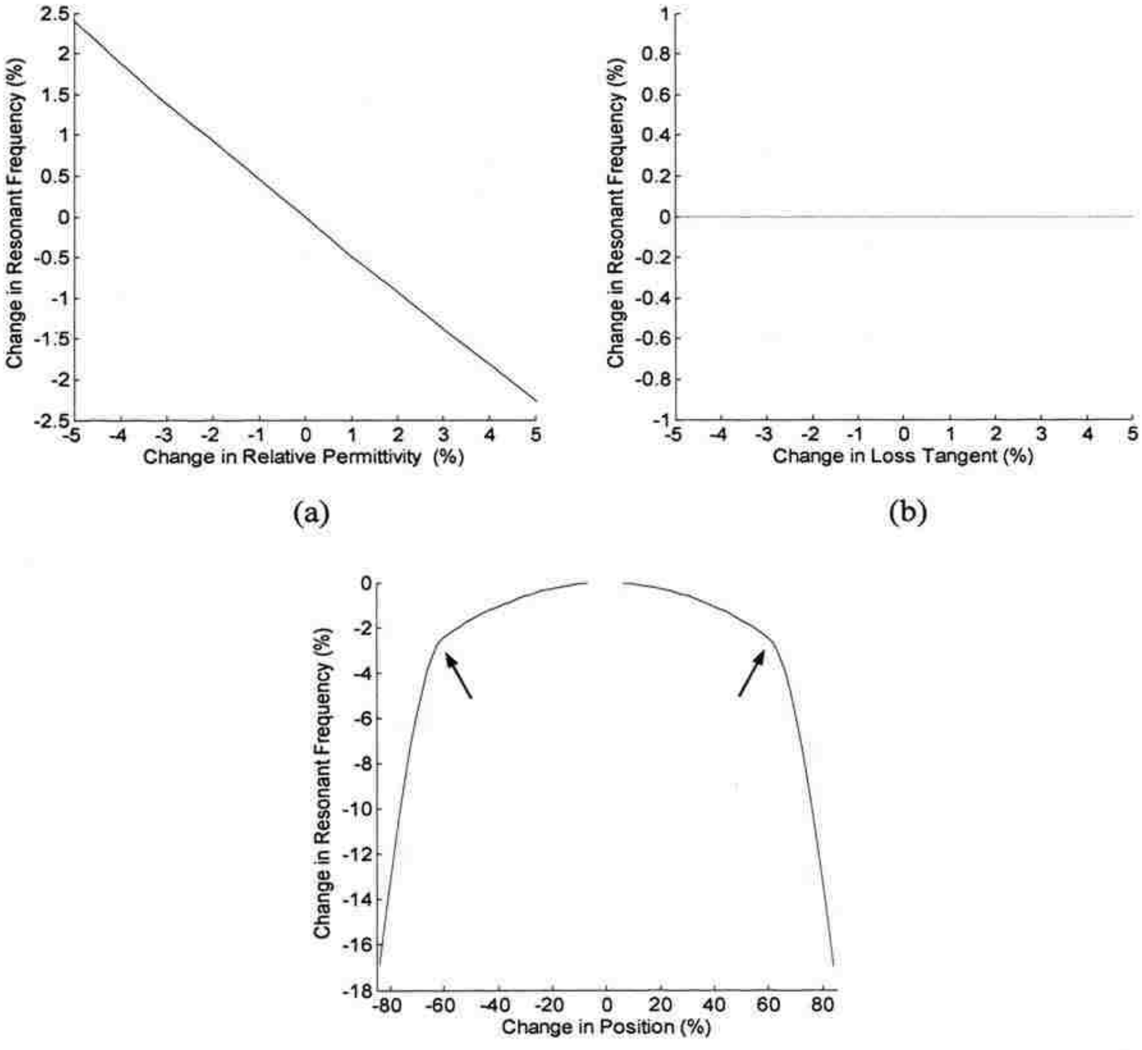

(a)

(b)

(c)

Figure 3.4. Simulated sensitivities of resonant frequency for cracks in aluminum plate with $D = 0.26$ mm and $W = 0.5$ mm at W-band and, except as perturbed for the analysis, filled with a dielectric of $\varepsilon_r' = 10$ and $\tan\delta = 0.06$: sensitivity to a) relative permittivity, b) loss tangent, and c) position of crack in waveguide aperture.

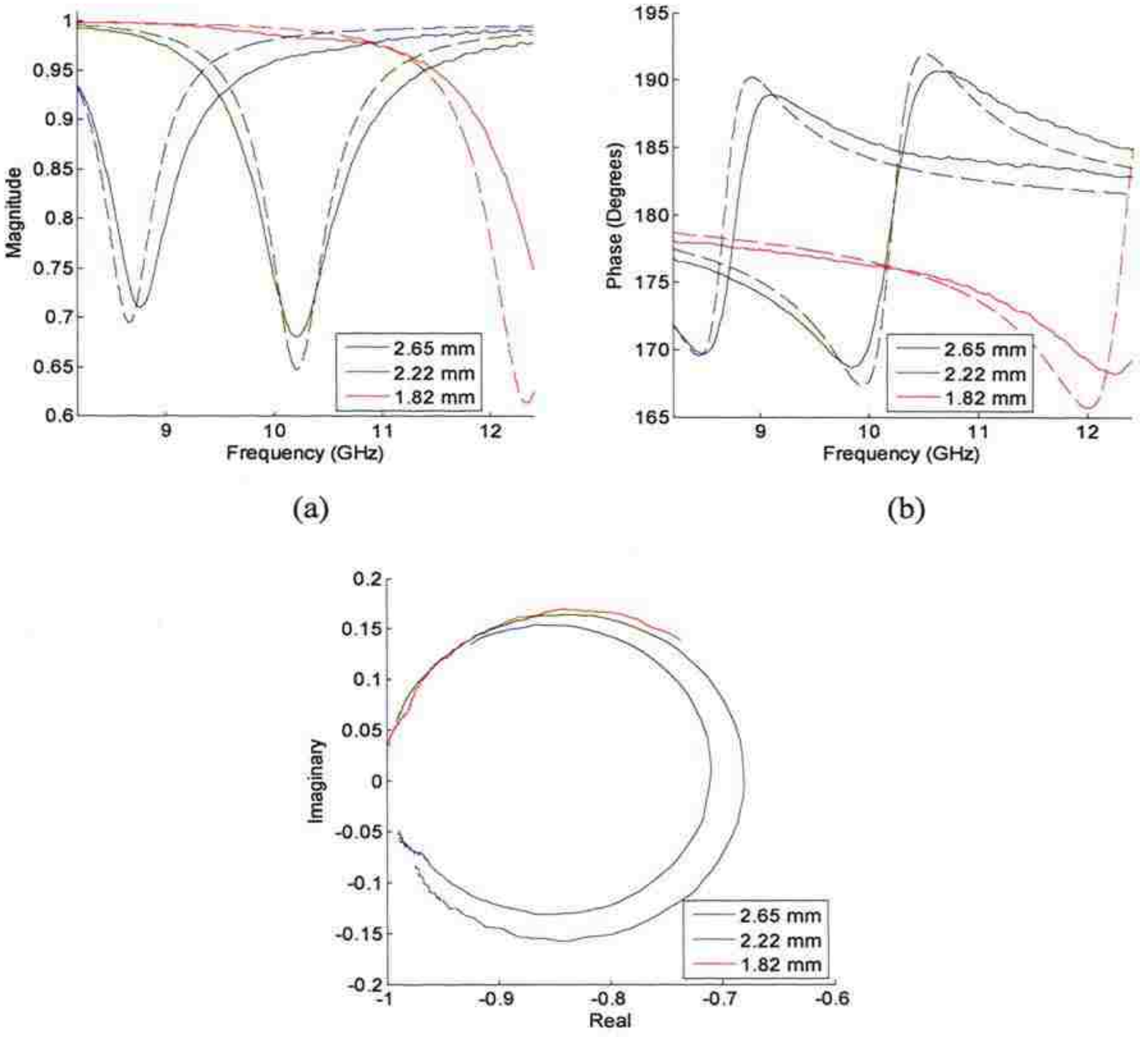

(a)

(b)

(c)

Figure 3.5. Measured (solid) and simulated (dashed) complex reflection coefficient of barium titanate-filled cracks in aluminum with $W = 0.5$ mm and three depths at X-band: a) magnitude and b) phase of the reflection coefficient as a function of frequency, and c) reflection coefficient in the complex polar plane.

effect and the trend between the resonant frequency and crack depth. Figure 3.6c shows the results in complex polar plane. The circular responses are again clearly evident and again the circles all cross the real axis ($\Gamma'' = 0$) to the left of the origin, though much closer to the origin than for the X-band measurements since b is smaller and these cracks are, thus, relatively wider. Consequently, it can be concluded that these cracks are also

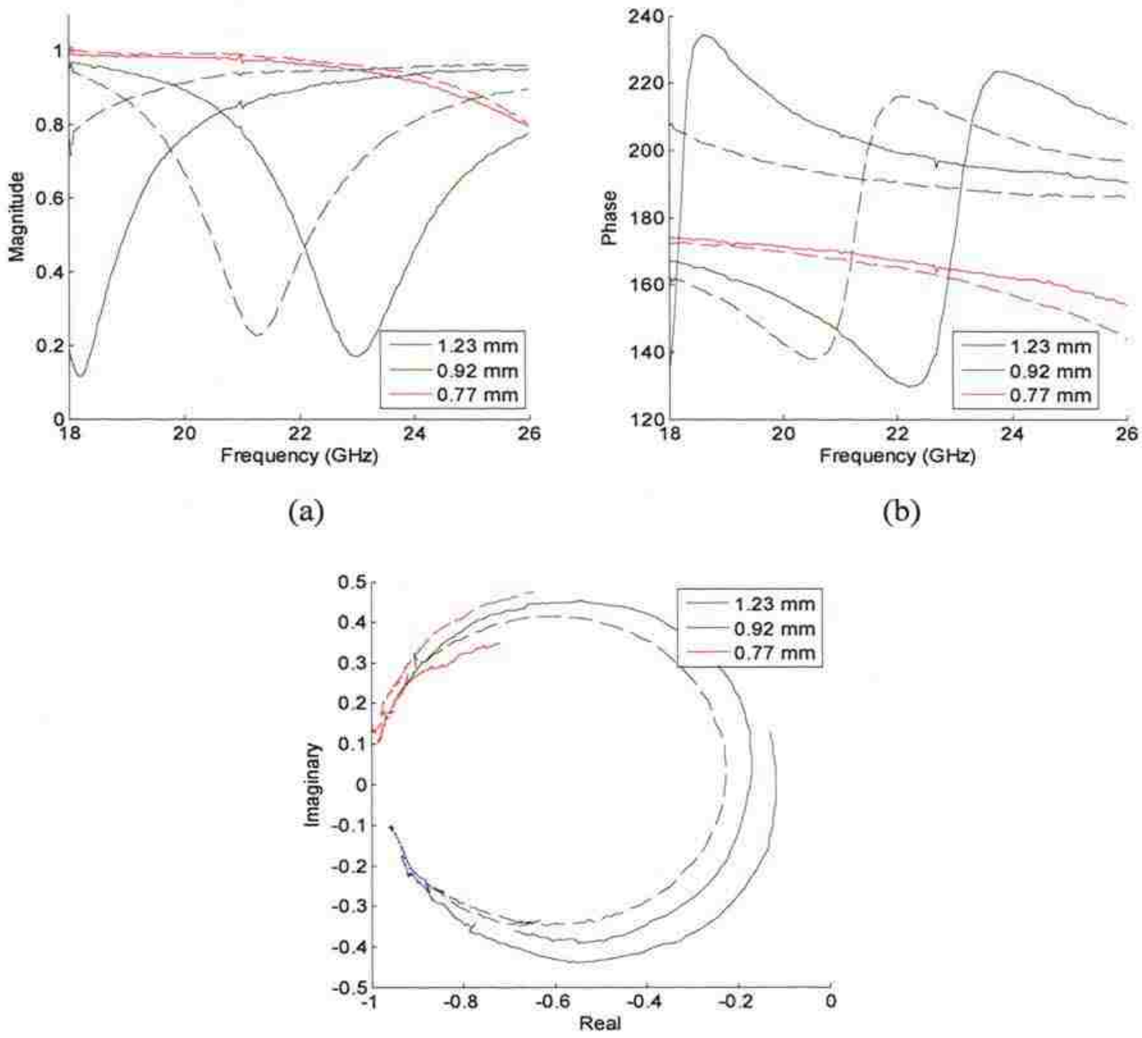

(a)

(b)

(c)

Figure 3.6. Two measurements (solid and dashed) of complex reflection coefficient of barium titanate-filled cracks in aluminum with $W = 0.85$ mm and three depths at K-band: a) magnitude and b) phase of the reflection coefficient as a function of frequency, and c) reflection coefficient in the complex polar plane.

undercoupled, but much nearer to critical coupling than the cracks measured at X-band, resulting in a somewhat larger magnitude dip and phase variation (compare to Figure 3.5a-b).

Figure 3.7 shows the resonant response for barium titanate-filled cracks at Ka-band, with respective depths of 0.74, 0.87, 0.88, and 1.19 mm and with $W = 0.5$ mm for the 0.88 mm-deep crack and $W = 0.85$ mm for the others. Figure 3.7a shows the simulated magnitude of reflection coefficient and Figure 3.7b shows the measured reflectometer output voltage (the reflectometer system and post-processing is explained in Section 1.3) so curves cannot be directly compared between the figures. However, the resonant frequency (at the signal minimum) and level of the minimum relative to the other cracks should be the same for both figures (these parameters are unchanged by the non-linear characteristics of the detector and the smoothing of the curves), and can be compared. There are also frequency dependencies introduced by imperfections of the reflectometer system, but the crack resonance can still be easily determined. The measured resonant frequency of the 1.19 mm-deep crack is shifted about 1 GHz (~3%) from simulation. The 0.87 and 0.88 mm-deep cracks are similarly shifted and their resonant frequencies remain close to one another, which is expected since even though there is a significant difference in widths the resonant frequency is primarily dependent on depth, and those are very close. It is also interesting to note that the difference in widths (and, consequently, coupling) is manifested in the different levels of the minima

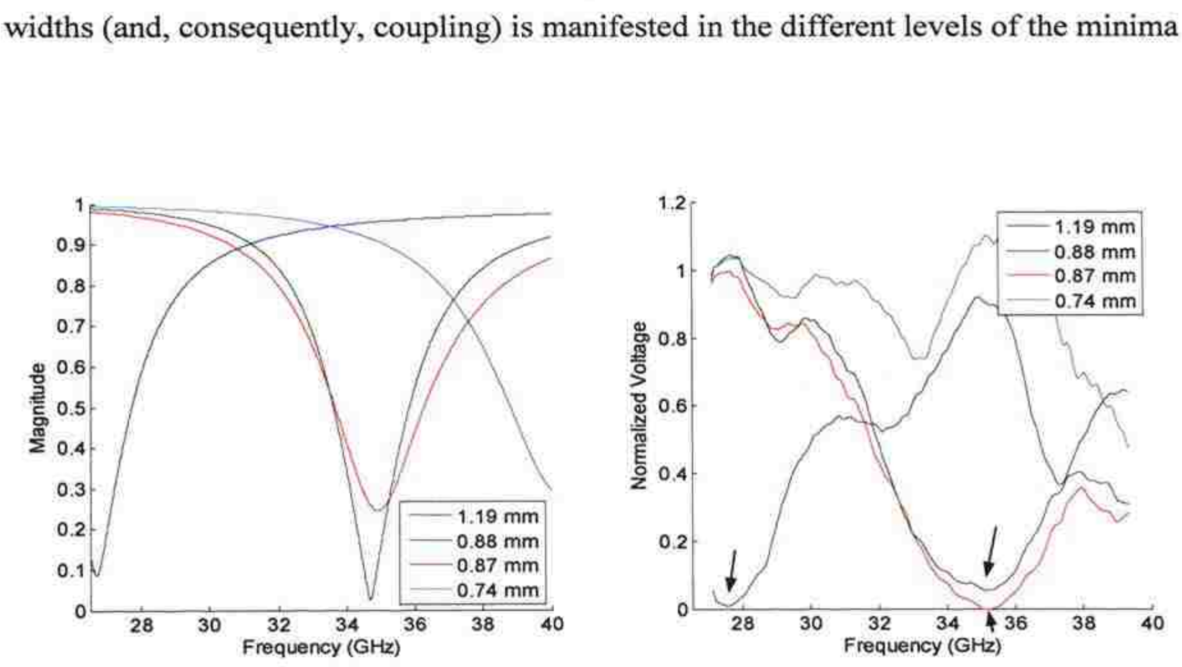

(a) (b)

Figure 3.7. Resonant response as a function of frequency for barium titanate-filled cracks with four depths at Ka-band: a) simulated magnitude of reflection coefficient and b) measured reflectometer output. The 0.88 mm-deep crack has $W = 0.5$ mm and all others have $W = 0.85$ mm. In b) smoothing and normalization to a no crack measurement (per frequency point) have been applied and the resonances are indicated by arrows.

dependency of the system. This curve has a wider resonant dip (i.e. lower Q-factor) than the other cracks, which would make it more sensitive to these frequency dependencies.

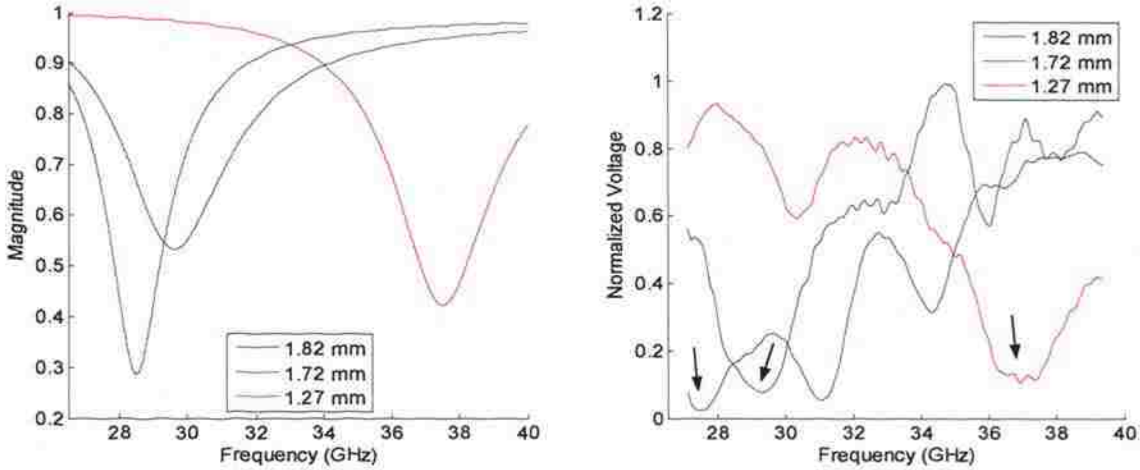

(a) (b)

Figure 3.8. Resonant response as a function of frequency for corn oil-filled cracks with three depths at Ka-band: a) simulated magnitude of reflection coefficient and b) measured reflectometer output. The 1.82 and 1.27 mm-deep cracks have $W = 0.5$ mm and the 1.72 mm-deep crack has $W = 0.85$ mm. Smoothing and normalization to a no crack measurement (per frequency point) have been applied in b), and the resonances are indicated by arrows.

Figure 3.9 shows the measured frequency dependence of the complex reflection coefficient for cracks with widths of 0.75, 1.13, and 1.5 mm and corresponding depths of 1.03, 1.01, and 0.99 mm, respectively, filled with distilled water at X-band. As expected, due to the high loss of the water, the change in magnitude and phase (Figures 3.9a-b) are small. Small frequency dependent measurement error (i.e., the ripples in the magnitude and phase) is also much more significant since the overall change is small. The resonant frequencies are close for the three samples, which is expected since the depths are similar. Figure 3.9c shows the results in complex polar plane. The circular responses are clearly evident and the circles cross the real axis ($\Gamma'' = 0$) well to the left of the origin,

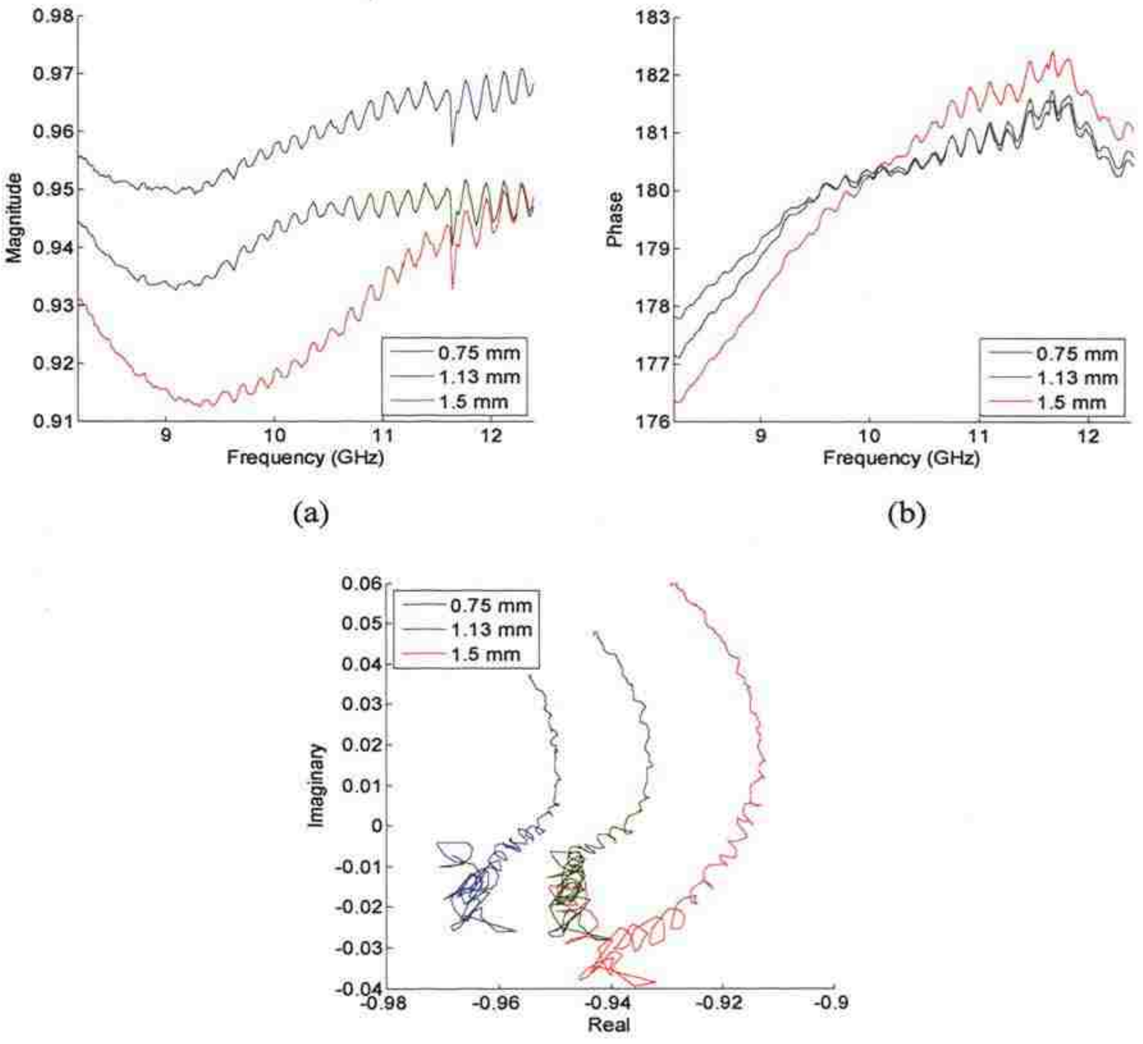

(a)

(b)

(c)

Figure 3.9. Measured complex reflection coefficient of distilled water-filled cracks in aluminum with widths of 0.75, 1.13, and 1.5 mm and corresponding depths of 1.03, 1.01, and 0.99 mm, respectively, at X-band: a) magnitude and b) phase of the reflection coefficient as a function of frequency, and c) reflection coefficient in the complex polar plane.

indicating that these cracks are highly undercoupled. The measurement error is again clearly seen due to the small overall change in the reflection coefficient.

Figure 3.10 shows a comparison of the estimated depth and the actual crack depth for simulations of cracks filled with barium titanate and measurements of cracks filled with barium titanate, corn oil, and distilled water. The dielectric properties given in Table 3.1 were used for the barium titanate in the simulations and the depth calculation for both simulations and measurements; a value of $\varepsilon_r' = 2.5$ [42] was used for the corn oil and a value of $\varepsilon_r' = 66$ [43] was used for the distilled water. For the simulations, a crack with $W = 0.5$ mm was used and the (actual) depth was varied. The measurements include a mix of cracks with widths from 0.5 to 1.5 mm, and the "actual depth" was measured by a micrometer. For both simulation and measurement the resonant frequencies were found from the minimum of the magnitude of reflection coefficient, and the depth was estimated using (2). Figure 3.10 clearly shows the ability of this method to reasonably accurately estimate crack depth. The depth estimation from simulation is quite accurate, with error of only a few percent coming from the crack width as described previously. Depth estimation using the measurements show greater error; especially for the K- and Ka-band barium titanate-filled crack measurements, which is most likely due to the

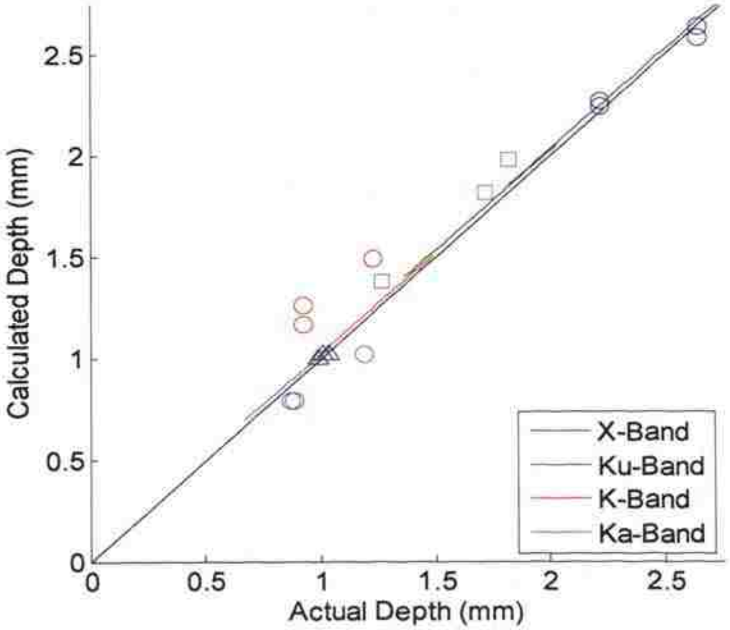

Figure 3.10. Comparison of depth calculated from simulation of barium titanate-filled cracks (lines) and measurement of barium titanate (circles), corn oil (squares), and distilled water (triangles) filled cracks using (2), to actual depth (as measured by micrometer). Repeated measurements of the same crack samples are included.

extrapolation of relative permittivity for these bands. The variations in packing also contribute to the error in barium titanate measurements, as can be seen in the difference between estimated depths for repeated measurements of the same crack. The influence of crack width on the resonant frequency may also be important, and since it was much greater for empty than filled cracks it will likely be greatest for small permittivity materials (e.g., corn oil). The positioning of the waveguide over the crack is another source of error common to the measurements.

Figure 3.11 shows a comparison of the estimated depth and the actual crack depth for the barium titanate-filled cracks in Figure 3.10, using (14) to correct for the crack width ((14) was derived for permittivities near barium titanate, and may not be accurate for the other filling materials). It is observed that for this case the depths calculated from simulation are very accurate, within 0.6% of the actual depths. The accuracy of depth estimation from measurement is not significantly changed, suggesting that other sources of error are more significant than the influence of crack width.

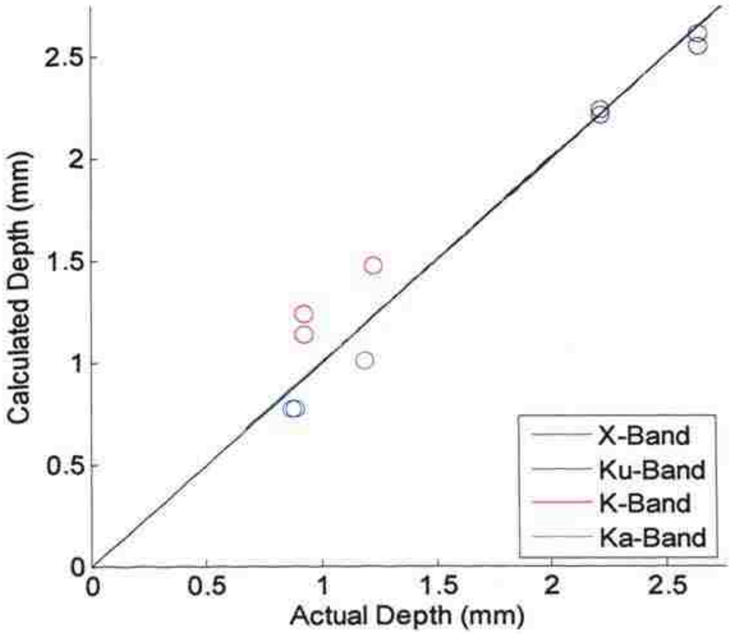

Figure 3.11. Comparison of depth calculated from simulation and measurement of barium titanate-filled cracks to actual depth, as shown in Figure 3.10 but corrected for width using (14).

3.2. FINITE CRACKS

As for finite empty cracks, the behavior of finite filled-cracks can be somewhat similar to long cracks if the crack length is sufficient to support a propagating mode for a portion of the frequencies within the band. Additionally, the filling material makes the cracks electromagnetically longer and the effect of reducing crack length is lessened, as will be shown.

Figure 3.12 shows the simulated frequency dependence of the complex reflection coefficient for cracks with $D = 3$ mm, $W = 2.3$ mm, and six different lengths (starting from $L = a = 23$ mm), filled with a dielectric ($\varepsilon_r = 9$, $\tan\delta = 0.063$) at X-band. It is seen in both the magnitude and phase that the resonant frequency shifts to the right (higher frequencies) as the crack length decreases, as happened for empty cracks and expected from (2). This shift accelerates as the length is reduced. The resonant frequency shifts slower for filled-cracks than for empty cracks; the resonance is still observed even when $L = 8$ mm ~ $a/3$, while for empty cracks it disappeared before $L = a/2$. It is also observed from both the magnitude and phase that the coupling is reduced as the length decreases, as expected since the 23 mm long crack is already undercoupled (from the phase,

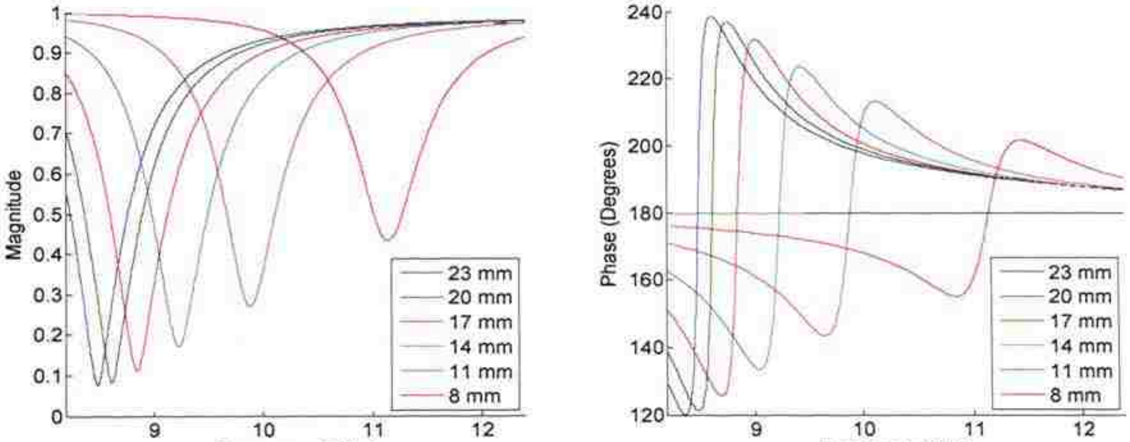

(a) (b)

Figure 3.12. Simulated complex reflection coefficient as a function of frequency for filled ($\varepsilon_r = 9$, $\tan\delta = 0.063$) finite cracks in perfect electric conductor with $D = 3$ mm, $W = 2.3$ mm, and six lengths at X-band: a) magnitude and b) phase.

compare to Figure 3.1b) and as the length is reduced even less signal will be coupled into the crack.

Figure 3.13 shows the effect of reduction in crack length from *a* on depth evaluation, for empty and filled-cracks with $W = 2.3$ mm and depths of 13 and 3 mm, respectively. The different depths were necessary to position the resonant frequency at approximately the same initial ($L = a$) value. Figure 3.13a shows the change in resonant frequency. Although a shift in the resonant frequency occurs in both cases, it is much less for filled than for empty cracks, as observed above, allowing shorter cracks to be evaluated. Figure 3.13b shows the error in depth evaluation using (2) as a function of reduction in crack length. These results suggest that crack depth could be reasonably estimated using (2) as long as the resonant frequency is within the frequency band and crack length is known. The error due to crack length could also be removed, using a correction factor as a function of crack length.

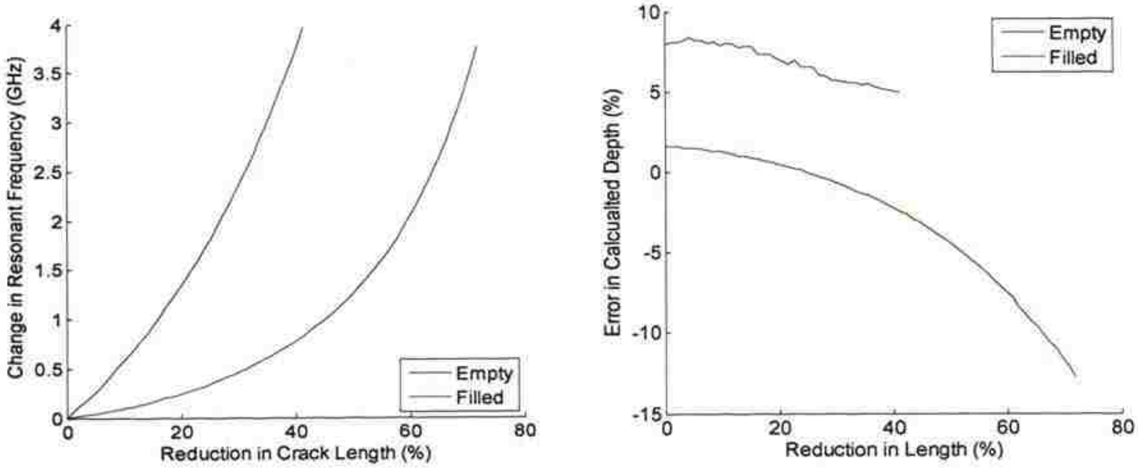

(a) (b)

Figure 3.13. Effect of reduction in crack length from *a* on depth evaluation for empty ($D = 13$ mm, $W = 2.3$ mm) and filled ($\varepsilon_r = 9$, $\tan\delta = 0.063$, $D = 3$ mm, $W = 2.3$ mm) cracks in perfect electric conductor at X-band: a) change in resonant frequency and b) error in depth estimation using (2).

3.3. PITS

Filled pits have electrically larger dimensions than when empty and may support propagating waves while being small enough to be contained in the probing waveguide aperture. Figure 3.14 shows the simulated magnitude of reflection coefficient and measured reflectometer output for four barium titanate-filled pits with diameter of 2.75 mm and four different depths at Ka-band. Resonances are clearly visible in the simulated magnitude for the three deepest pits, as seen in Figure 3.14a, and a part of the resonant dip is visible for the shallowest pit. This shows that these pits will support at least one propagating mode. The edge of the resonant dip for a second resonance is also visible for the 2.51 mm-deep pit. Simulations (not shown) indicated that these pits will support at least two propagating modes which are excited by the probing waveguide. Consequently, the pit depth cannot be calculated directly from equations for circular waveguides and the relationship would likely have to be developed from simulation or measurement. Figure 3.14b shows measurement results for pits with similar dimensions using the Ka-band reflectometer. As for the simulations, resonances are visible for the three deepest cracks,

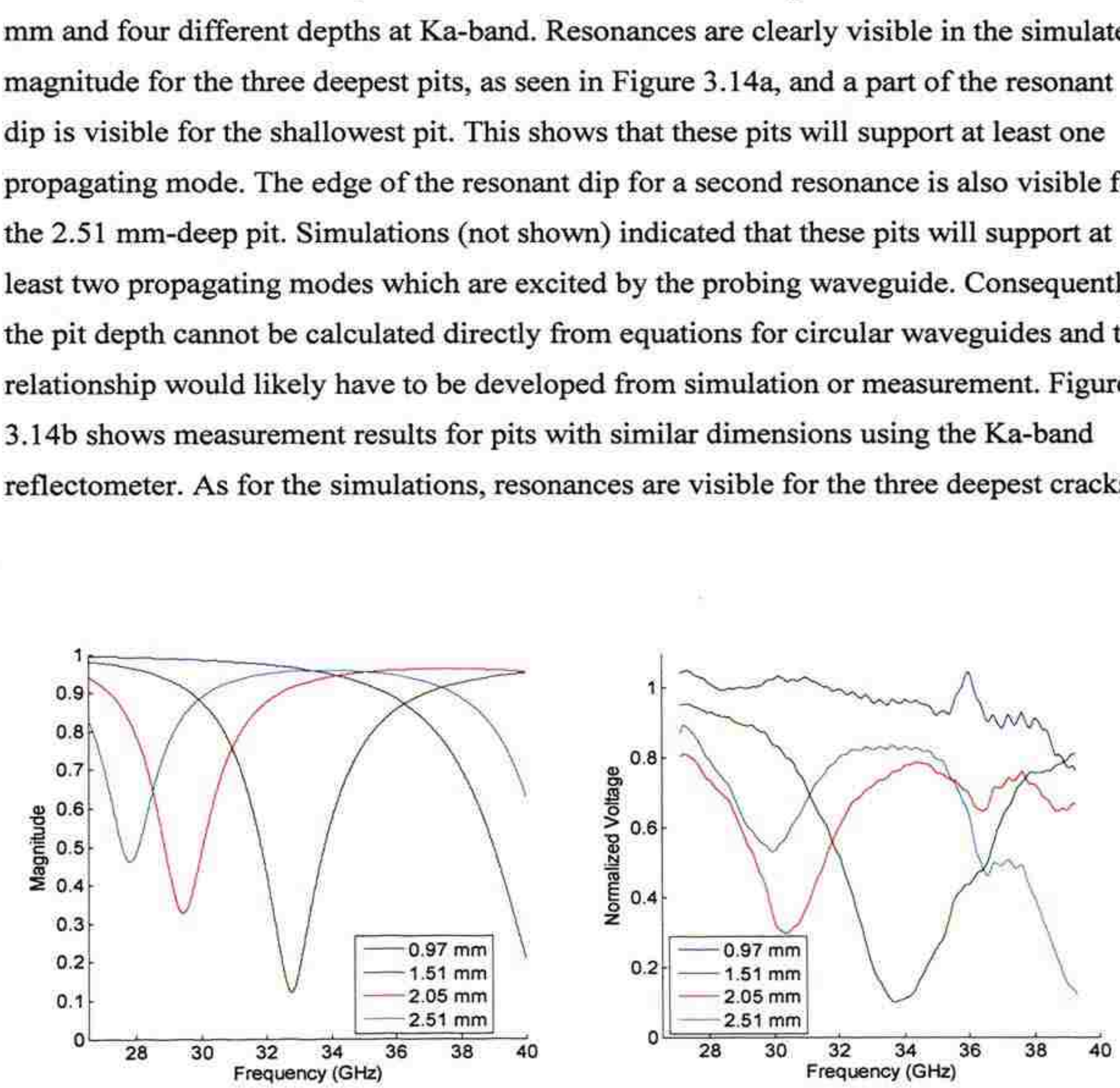

(a) (b)

Figure 3.14. Resonant response as a function of frequency for barium titanate-filled cracks with diameter of 2.75 mm and five depths at Ka-band: a) simulated magnitude of reflection coefficient and b) measured reflectometer output. In b) smoothing and normalization to a no crack measurement (per frequency point) were applied.

and a part of the resonance response is seen for the shallowest. The edge of the second resonant dip is seen for the 2.51 mm-deep crack as well and, in fact, shows a greater drop in signal.

4. DIELECTRIC SLAB-LOADED WAVEGUIDE PROBE

4.1. PROBE DESIGN

The quarter-wavelength method of depth evaluation presented in Sections 2 and 3 has a practical limitation which is the requirement of using high frequencies for very shallow damage depth to become equal to a quarter-wavelength. It is also limited by the requirement that damage length or diameter is large enough to support a propagating mode. A probe was designed to avoid these limitations by providing a resonance within the probe itself. The probe is placed so that the sample being tested (conducting plate and damage) becomes one face of the resonator. Damage in the sample may change the response of the resonance, and analysis of these changes may allow evaluation of the damage depth.

The resonant structure was formed by placing a dielectric insert in the probing waveguide, as shown in Figure 4.1. The shape of the insert is shown in Figure 4.1a. A dielectric insert of this shape has been used before to concentrate the electric field in the center of the waveguide and increase its sensitivity for detecting tiny pits [30] in a non-resonant measurement approach. The dielectric material TMM10I, a ceramic polymer composite designed for stripline and microstrip applications, was used for the insert. The dielectric properties of this material are listed to be $\varepsilon_r' = 9.8 \pm 0.245$ and $\tan\delta = 0.002$ [46] and it can be purchased in a sheet form which readily enables cutting it to the desired

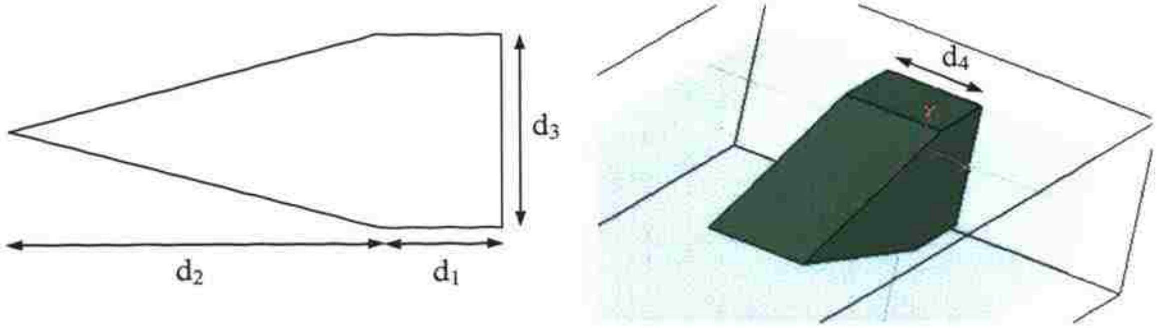

(a) (b)

Figure 4.1. Dielectric insert: a) Side-view and b) perspective view in waveguide (to-scale). $d_1 = 2.5$ mm, $d_2 = 7.5$ mm, $d_3 = 4.3$ mm, and $d_4 = 3.175$ mm.

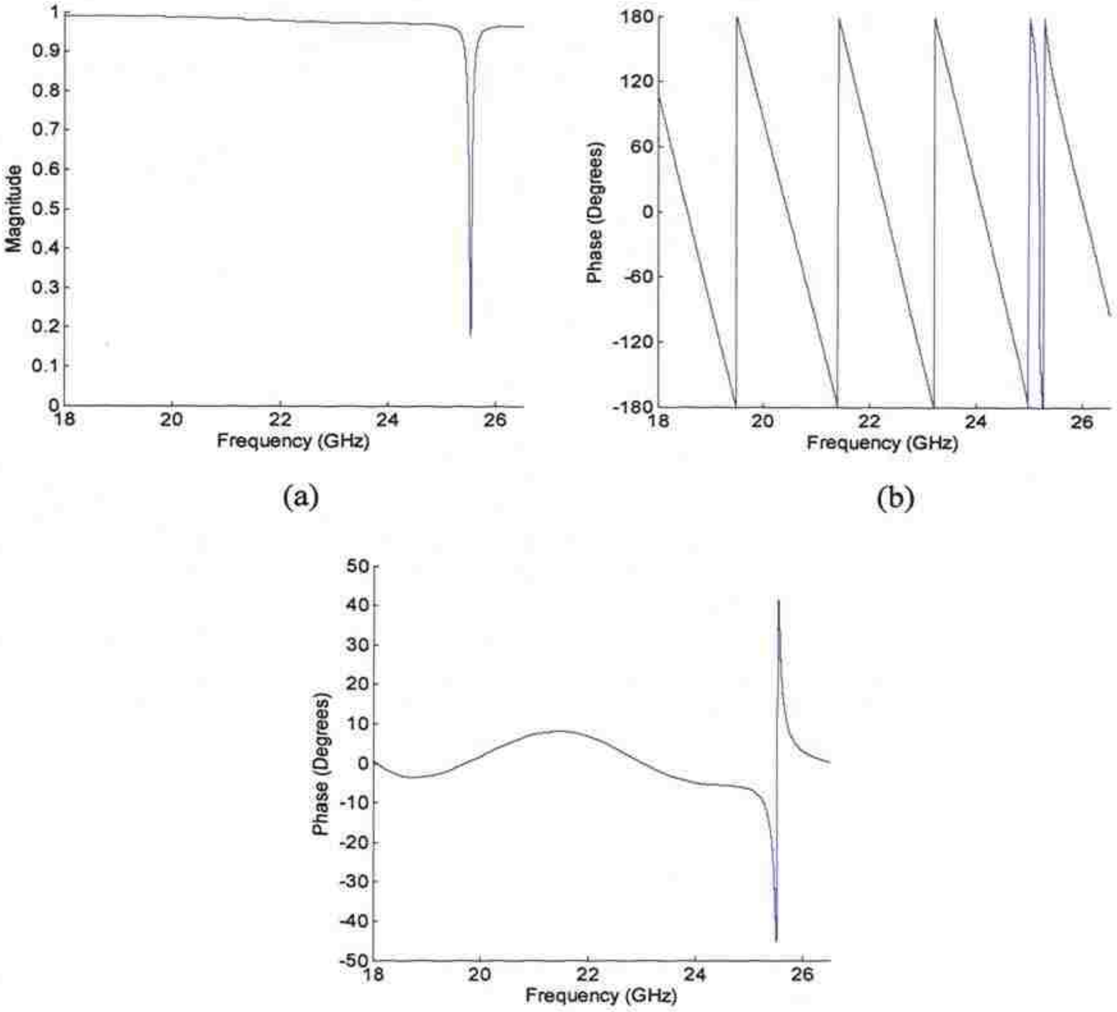

(a)

(b)

(c)

Figure 4.2. Simulated complex reflection coefficient as a function of frequency for slab-loaded waveguide probe and aluminum plate at K-band: a) magnitude, b) uncorrected phase, and c) corrected phase.

waveguide into quarter-wavelength resonant cracks in Sections 2 and 3. The minimums then correspond to critical coupling. This shows that d_1, d_2, and d_3 each affect the coupling from the empty waveguide into the resonant section of the probe. The noise-like variation in Figure 4.3d is due to the discrete frequency steps and does not reflect any physical phenomenon. For all of these cases the magnitude dips to less than 0.4 and, consequently, the resonant frequency can be easily determined from the magnitude.

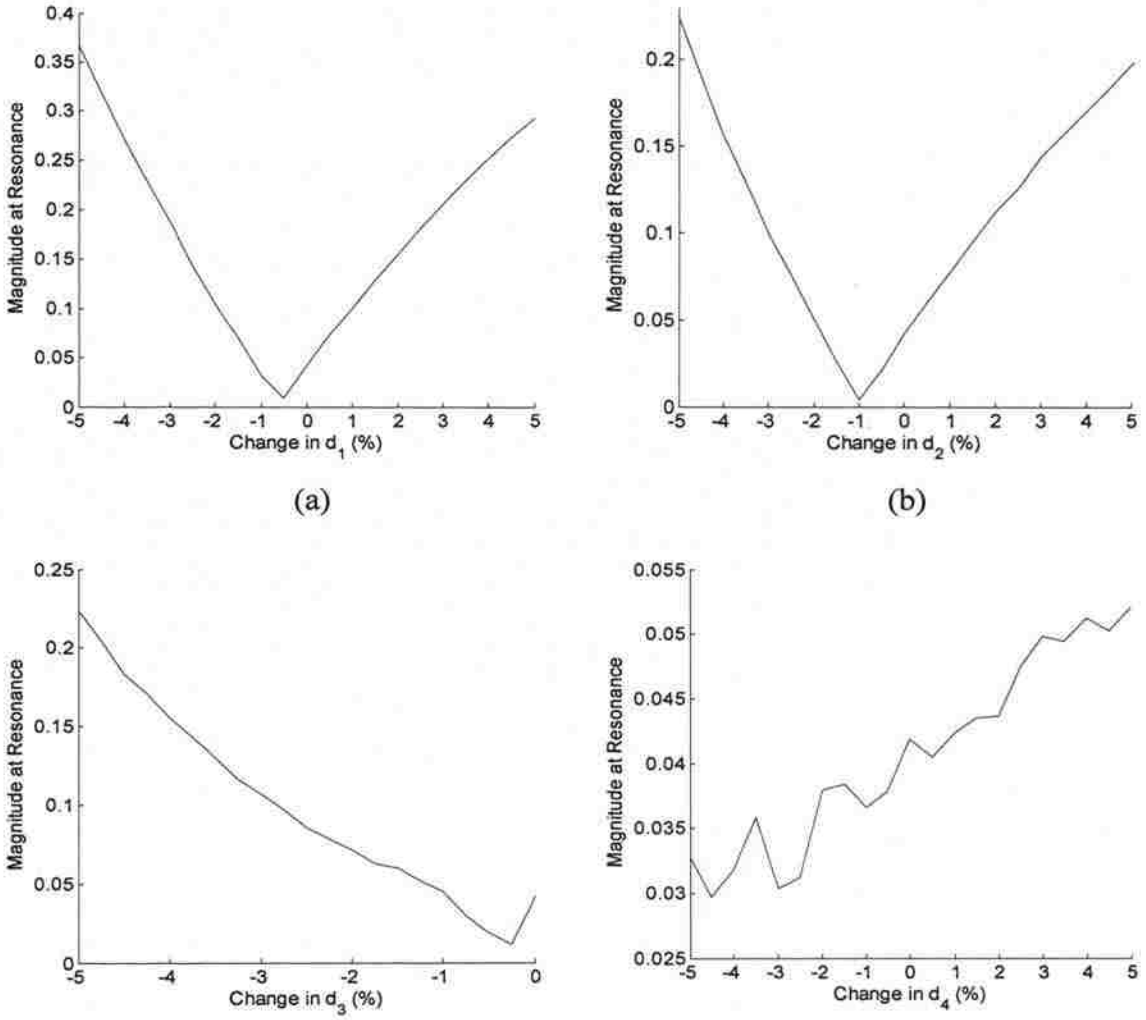

(a) (b)

(c) (d)

Figure 4.3. Simulated sensitivity of the magnitude level at resonance to geometric parameters of the dielectric insert at K-band: sensitivity to a) d_1, b) d_2, c) d_3, and d) d_4.

Figure 4.4 shows the simulated sensitivity of the resonant frequency to various geometrical parameters of the dielectric slab, as given in Figure 4.1. The resonant frequency is inversely related, in a near-linear fashion, to each parameter. This makes physical sense, since smaller resonators will tend to resonate at higher frequencies. The resonant frequency is most strongly dependent on d_3, with a 5% reduction resulting in a 1.6% shift of the resonant frequency. It is then dependent, in decreasing order of dependence, on d_4, d_1, and d_2, respectively. A shift in the resonant frequency due to the probe characteristics is not particularly critical since it will be common for reference and damage measurements. The shift may be significant if a direct comparison of simulation and measurement is desired or if the shift is large enough to move the resonance outside of the operating frequency band. These shifts are relatively small so the latter is not expected to occur.

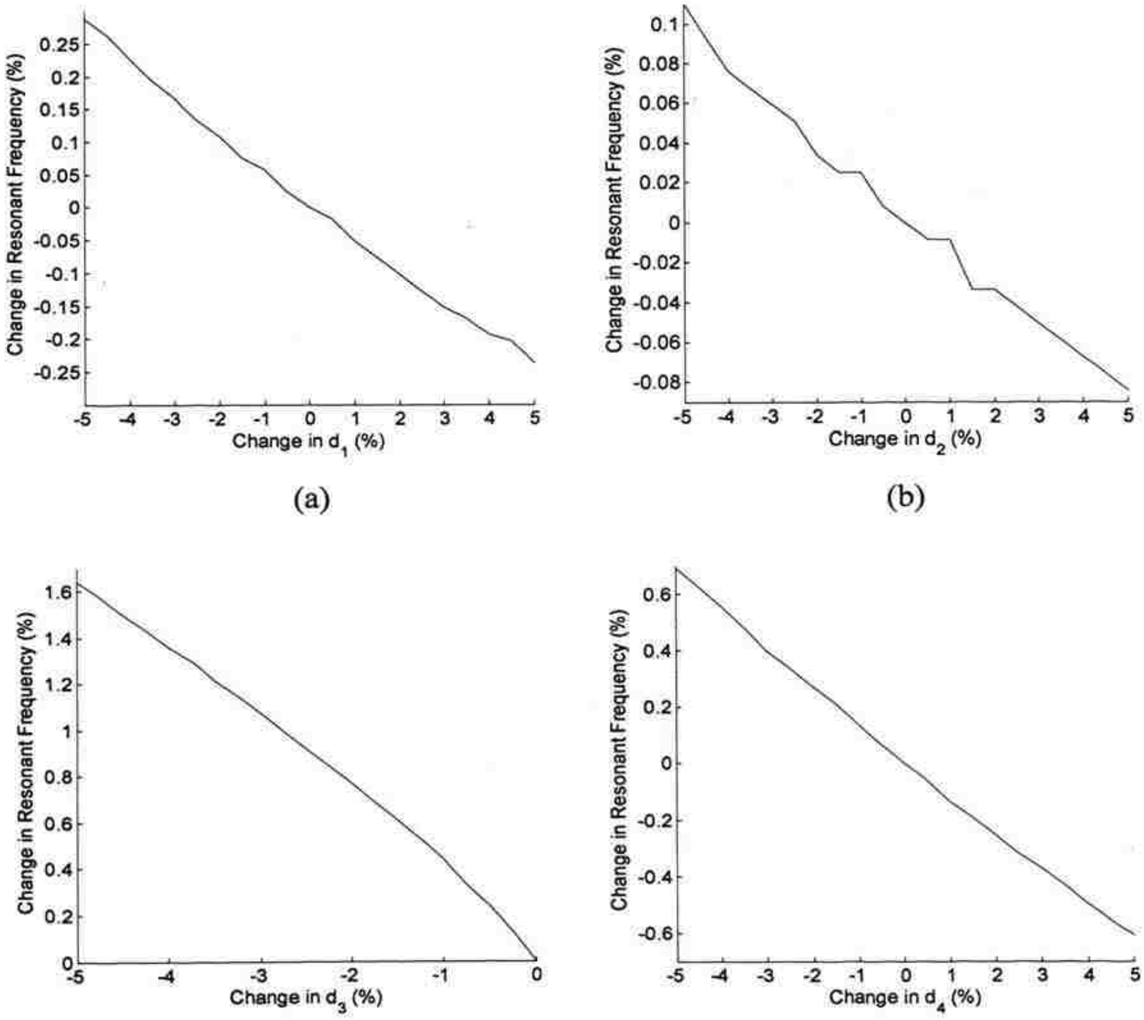

(a) (b)

(c) (d)

Figure 4.4. Simulated sensitivity of the resonant frequency to geometric parameters of the dielectric insert at K-band: sensitivity to a) d_1, b) d_2, c) d_3, and d) d_4.

4.2. LONG CRACKS

4.2.1. Simulation Results. The consideration of crack lengths extending beyond the waveguide aperture has a significant effect on simulation time and also whether crack length must be considered as a parameter to describe a "long" crack. Figure 4.5 shows the magnitude of reflection coefficient for long cracks with $D = 0.2$ mm, $W = 0.5$ mm and three lengths at K-band. The curves lie on top of one another, with virtually no difference in the reflection coefficient characteristics as a function of crack length. This shows that the reflection coefficient is not sensitive to crack length extending outside the probing waveguide aperture and the simulation geometry can be simplified by setting $L = a$, as shown in Figure 1.1a. This is expected since one of the consequences of the dielectric insert is that the electric field is concentrated in the center of the waveguide, resulting in this probe being less sensitive to variations in crack length than the empty waveguide probes described previously.

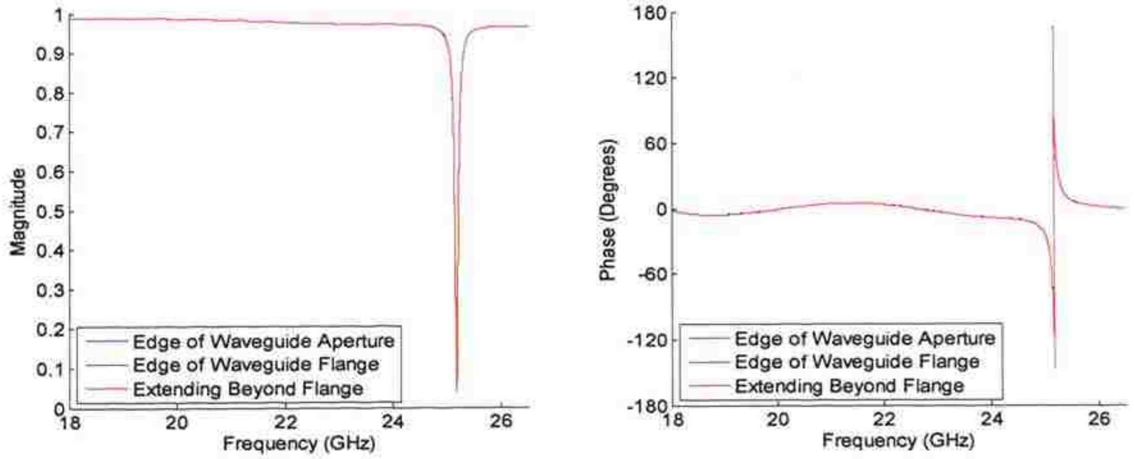

(a) (b)

Figure 4.5. Simulated complex reflection coefficient as a function of frequency for slab-loaded waveguide probe and crack in aluminum with $D = 0.2$ mm, $W = 0.5$ mm and three lengths at K-band: a) magnitude and b) phase.

Figure 4.6 similarly shows the complex reflection coefficient for cracks with $W = 0.5$ mm and six different depths at K-band, while crack lengths were set to be equal to a.

There is an obvious shift in the resonant frequency as a function of depth in both the magnitude and phase of reflection coefficient, with deeper cracks shifting the resonance further to the left (lower frequencies). There is also a non-monotonic change in the magnitude levels at resonance. If the phase is considered, it can be seen that as the crack depth increases the resonance behavior changes from undercoupled to overcoupled (phase change of less than 360° to phase change of 360°).

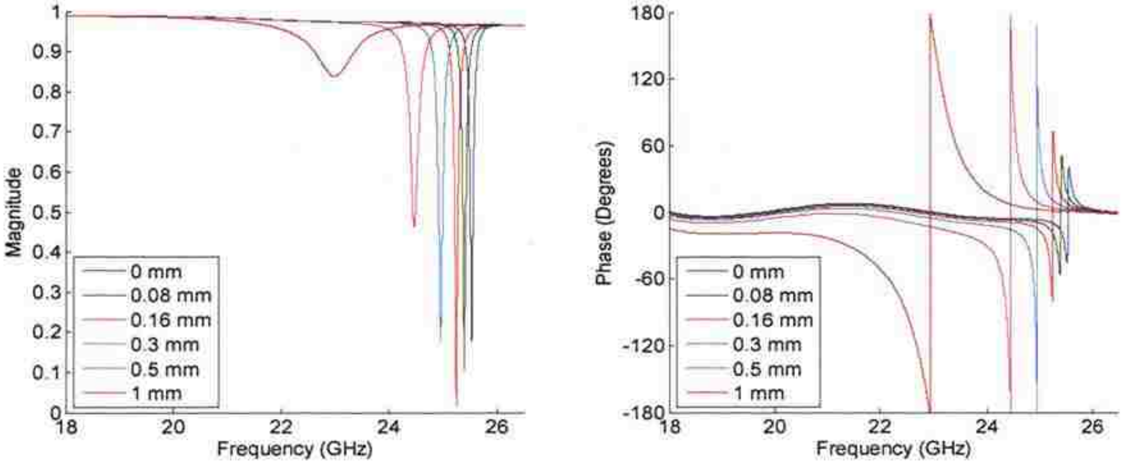

(a) (b)

Figure 4.6. Simulated complex reflection coefficient as a function of frequency for slab-loaded waveguide probe and cracks in aluminum with $W = 0.5$ mm and six depths at K-band: a) magnitude and b) phase.

Figure 4.7 shows simulated characteristics of the resonant response as functions of depth for four crack widths at K-band. Figure 4.7a shows the magnitude of reflection coefficient at the resonant frequency (i.e. magnitude minimum). A non-monotonic behavior is observed, similar to the results shown in Figures 2.4a and 3.2a, with the minimum indicating critical coupling. Figure 4.7b shows the resonant frequency and it is evident that for each width the resonant frequency can be related to a specific depth, which is a very significant feature for depth evaluation. The *Q*-factors shown in Figure 4.7c are much higher than those seen for crack resonators (see Figures 2.4b and 3.2b), which may allow more accurate determination of the resonant frequency. For each of these curves, as the depth increases the Q-factor smoothly decreases, with a distinct change in slope at one point (indicated by arrows). By comparison with Figure 4.7a these points correspond to critical coupling. Similar behavior was observed for filled cracks and is shown in Figure 3.2b. A quantization-like feature for the higher Q-factor values is

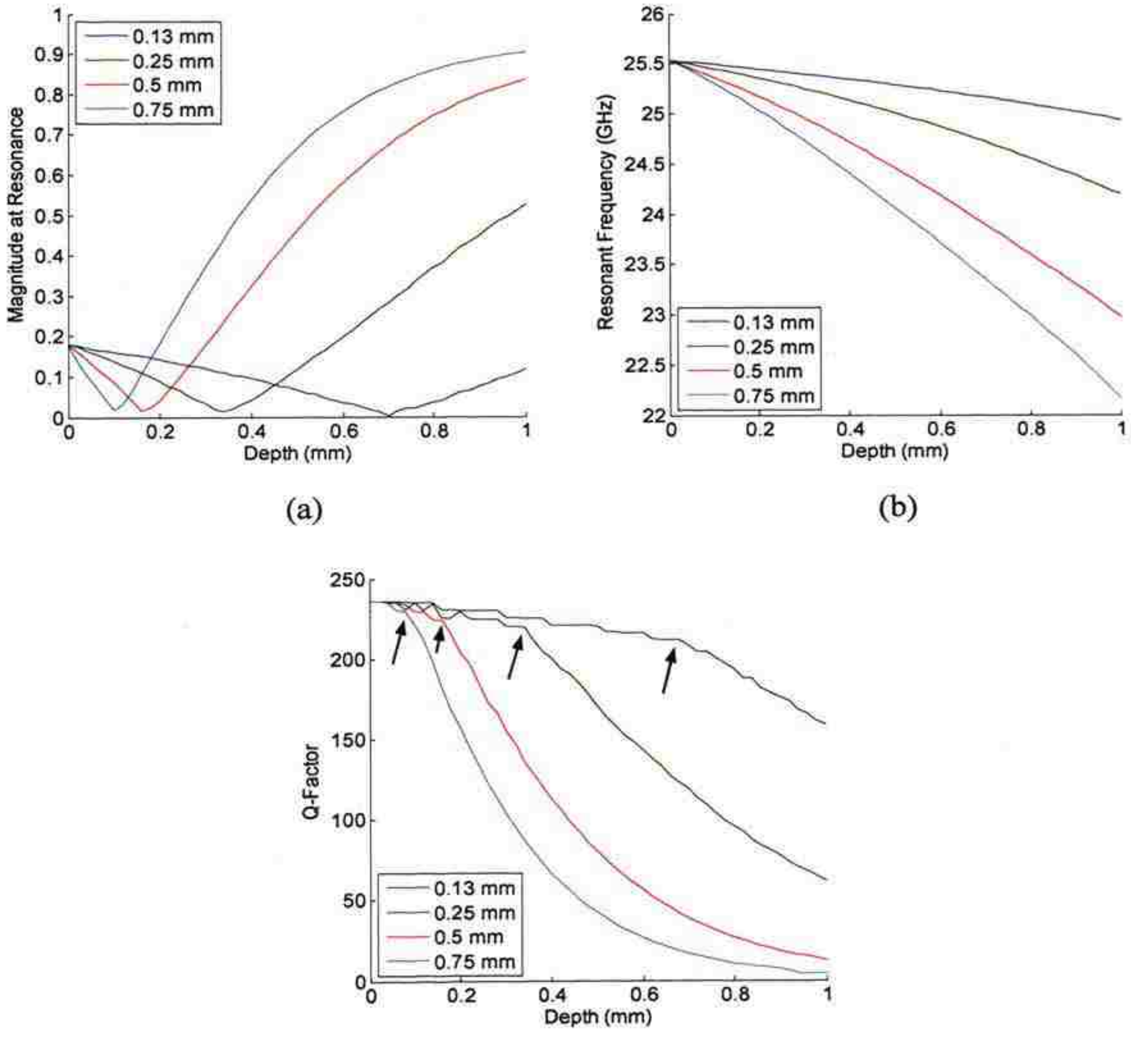

(a) (b)

(c)

Figure 4.7. Simulated characteristics of resonant response as a function of depth for slab-loaded waveguide probe and cracks in aluminum with four widths at K-band: a) magnitude of reflection coefficient at resonant frequency, b) resonant frequency, and c) Q-factor.

seen in Figure 4.7c, which is due to the fact that discrete frequency points were calculated in these simulation.

4.2.2. Sensitivity Analysis. The sensitivity of this method to variations in the probe position was investigated as well. Figure 4.8 shows the resonant response for a

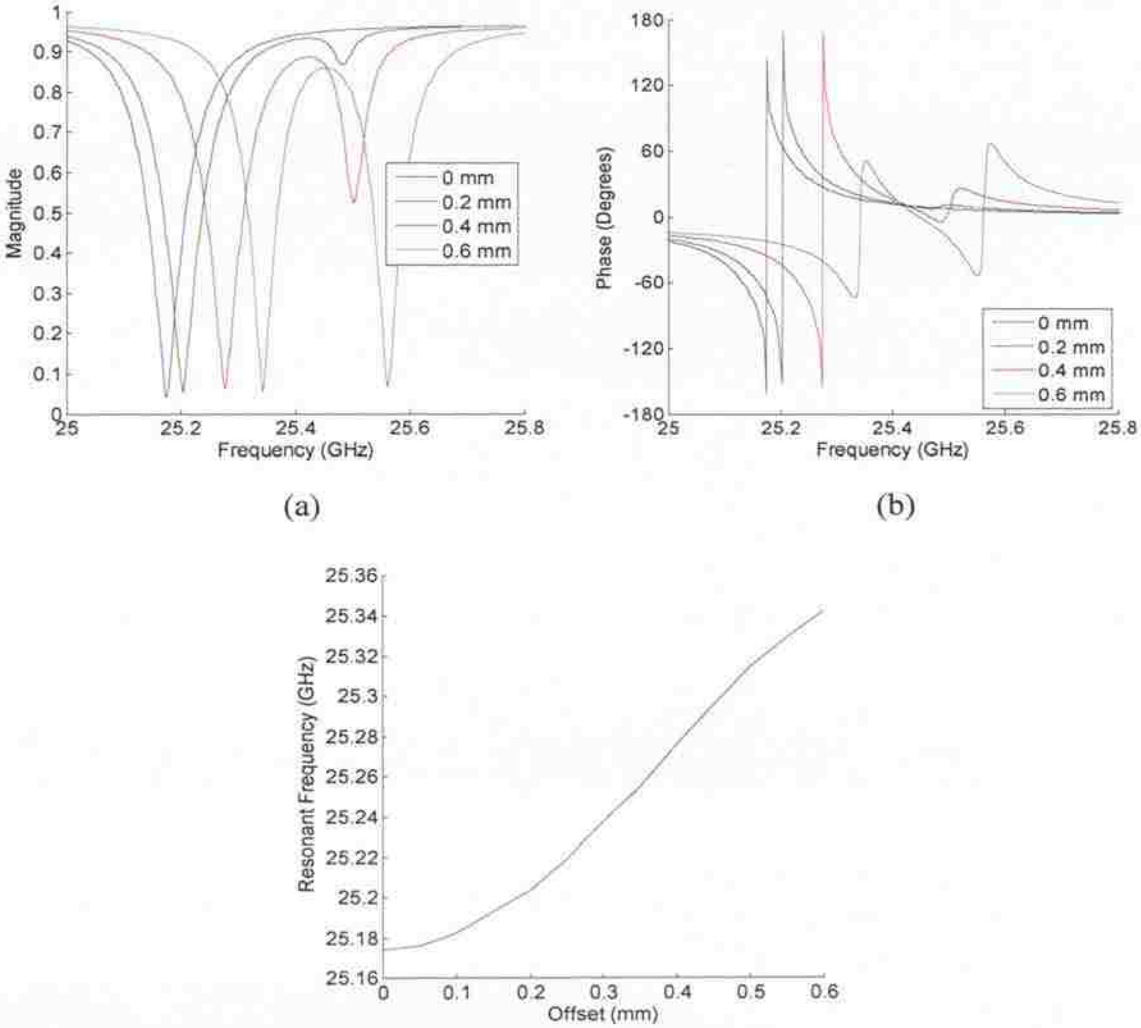

(a)

(b)

(c)

Figure 4.8. Simulated resonant response for slab-loaded waveguide probe and cracks in aluminum with $D = 0.2$ mm and $W = 0.5$ mm with its position varied along b from the center of the probe at K-band: a) magnitude and b) phase of reflection coefficient as a function of frequency for four position offsets and c) resonant frequency as a function of offset.

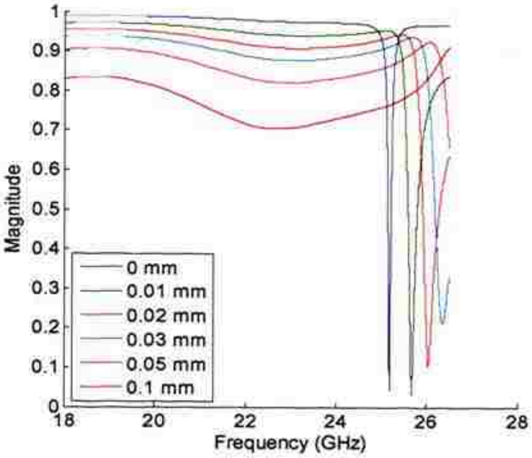

Figure 4.9. Simulated magnitude of reflection coefficient as a function of frequency for slab-loaded waveguide probe and crack in aluminum with $D = 0.2$ mm, $W = 0.5$ mm, and four liftoffs of the probe from the aluminum plate at K-band.

shallower than 0.2 mm (i.e., undercoupled cracks, from Figure 4.6b) filling the crack does not affect the magnitude at resonance significantly; but for deeper cracks the magnitude level is lower for filled cracks, and begins to decrease as a function of depth for depths of 0.7–1 mm. This is likely due to the loss from the dielectric in the crack. Figure 4.10b shows the resonant frequency. For depths less than 0.2 mm filling has no effect on the resonant frequency, but for deeper cracks the frequency shift is greater for filled cracks than for empty ones. Figure 4.10c shows that the *Q*-factor is also unchanged for depths less than 0.2 mm, but for greater depths the *Q*-factor is lower for filled cracks. This is expected since additional losses are introduced by the dielectric filling material. These simulations show that dielectric fillings have no effect for the shallowest cracks, the most important and difficult case for evaluation. However, for deeper cracks, a dielectric filling material may be beneficial for increasing the shift of the resonant frequency and the magnitude dip, at the cost of a lower *Q*-factor.

4.2.4. Measurement Results. A dielectric slab-loaded waveguide probe was prepared as shown in Figure 4.1. Figure 4.11 shows the magnitude of reflection coefficient for cracks with four different widths and various depths. Several resonances are observed; the desired resonance is indicated by the arrows and the resonant behavior is much wider (i.e., lower *Q*-factor) and has a smaller magnitude dip than predicted by

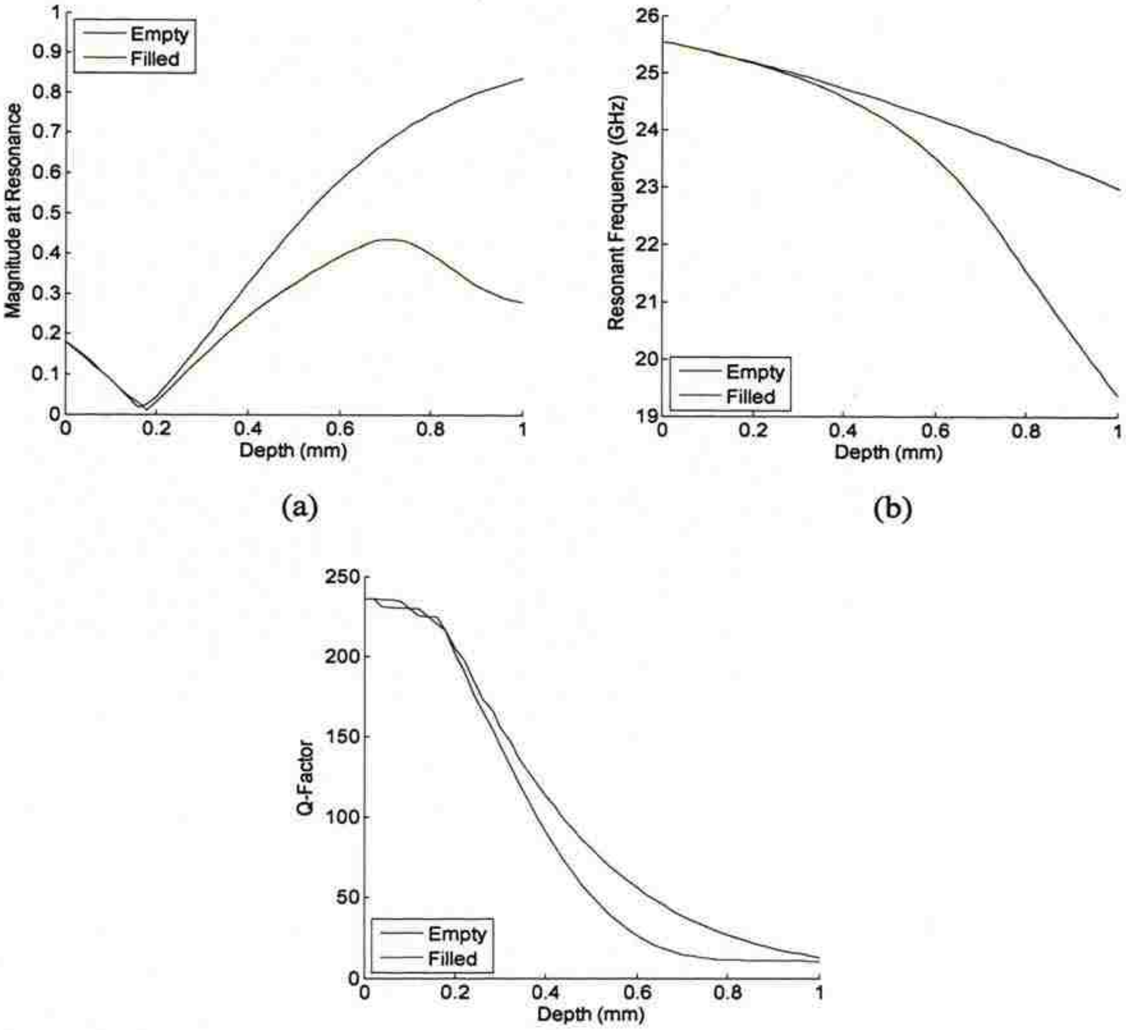

(a)

(b)

(c)

Figure 4.10. Simulated characteristics of resonant response as functions of depth for slab-loaded waveguide probe and empty and filled ($\varepsilon_r' = 10$, $\tan \delta = 0.06$) cracks in aluminum with $W = 0.5$ mm at K-band: a) magnitude at resonant frequency, b) resonant frequency, and c) *Q*-factor.

simulation. The additional resonances are most likely due to imperfections in the preparation and placement of the dielectric insert. The dominant resonance can easily be identified and the resonance frequency is observed to shift with depth, so some degree of depth evaluation may be possible. It is also worth noting that the magnitude level outside the resonance is much lower than shown by the simulation results (i.e., about 0.7 instead

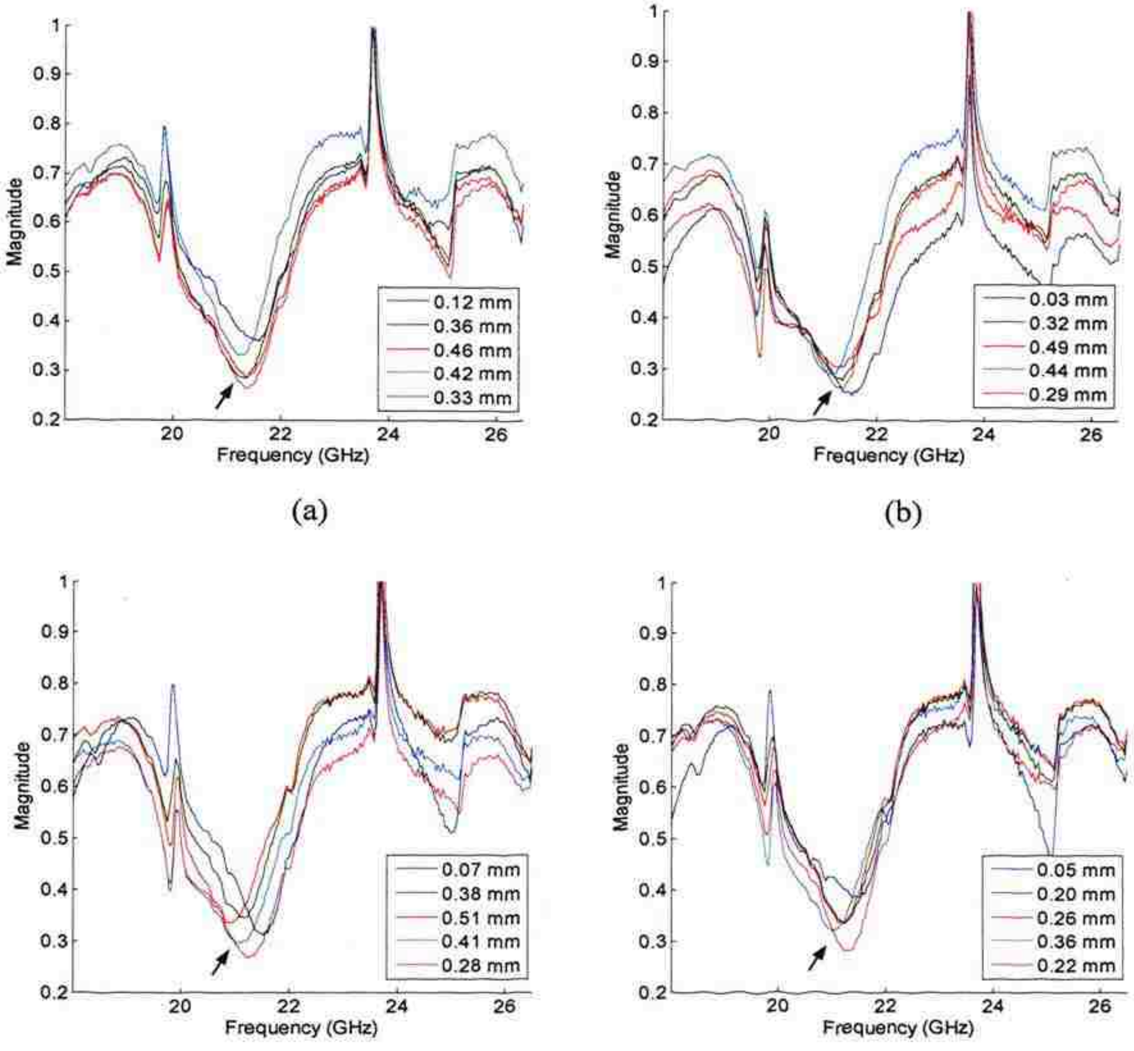

(a) (b)

(c) (d)

Figure 4.11. Measured magnitude of reflection coefficient as a function of frequency for slab-loaded waveguide probe and cracks with four widths and several depths at K-band: a) $W = 0.51$ mm and five depths, b) $W = 1.02$ mm and five depths, c) $W = 1.52$ mm and five depths, and d) $W = 2.54$ mm and five depths. The desired resonances are indicated by arrows.

of 0.95), which seems to indicate that there are significantly more non-resonance losses in the actual probe than there were in the simulations.

Figure 4.12 shows the resonant frequency, from the measurements in Figure 4.11, as a function of varying crack depth. The results show lower resonant frequencies for deeper cracks, as expected. However, the correlation is weak, which may be due to error from the imperfections in the probe construction or variations in probe position. If a few outliers are removed, these results suggest that crack depth may be evaluated with roughly 25% error.

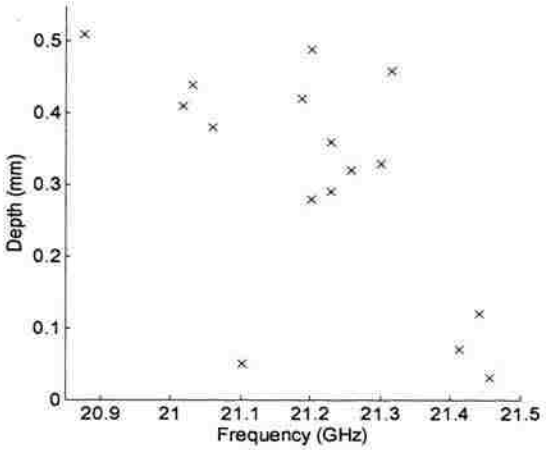

Figure 4.12. Crack depth vs. resonant frequency for slab-loaded waveguide probe and cracks with four widths at K-band.

A second probe was prepared and used to repeat the measurements of the 1.52 and 2.54 mm-wide cracks. Figure 4.13 shows the magnitude of reflection coefficient for these measurements, and can be directly compared to Figures 4.11c-d. It is observed that there are fewer extra resonances in these measurements, and those extra resonances are smaller, which may indicate that this probe was prepared more accurately. The desired resonance is clearly evident, and the resonant frequency shifts with crack depth. The resonant dip in magnitude is still smaller and wider (lower *Q*-factor) than expected from simulation, but the resonant frequency can still be easily determined. A second resonance is observed to the right of the desired resonant frequency, which is likely due to the offset of the probe position from the center of the crack (see Figure 4.8a).

Figure 4.14 shows the resonant frequency, from the measurements shown in Figures 4.13a-b, as a function of crack depth. The relationship between crack depth and

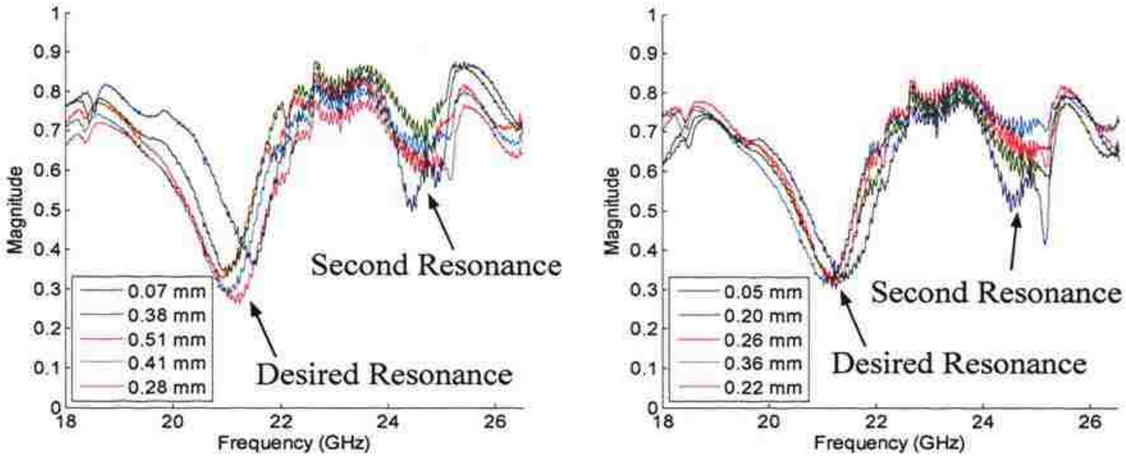

(a) (b)

Figure 4.13. Measured magnitude of reflection coefficient as a function of frequency for dielectric slab-loaded waveguide probe and cracks with two widths and several depths at K-band: a) *W* = 1.52 mm and five depths and b) *W* = 2.54 mm and five depths.

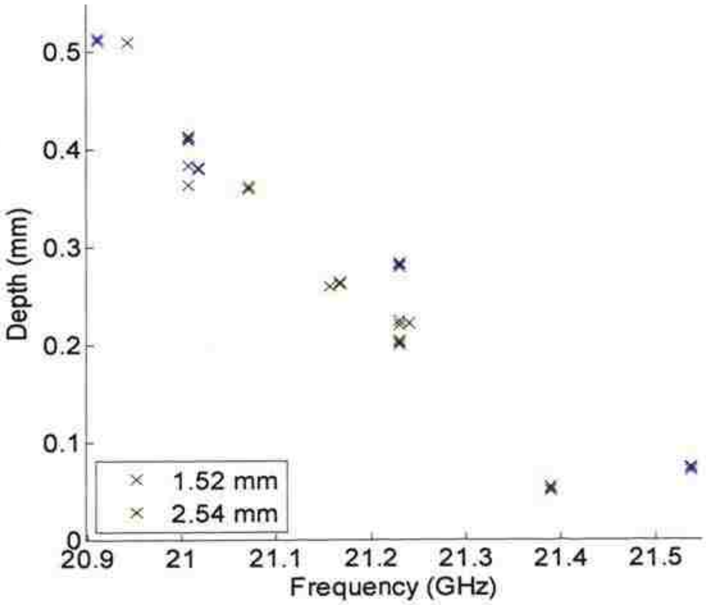

Figure 4.14. Crack depth vs. resonant frequency for slab-loaded waveguide probe and cracks with two widths at K-band. Three measurements of each crack are shown.

resonant frequency is much more clear for this set of measurements than those shown in Figure 4.12. The crack width is also seen to have an effect on the resonant frequency, with a roughly linear relationship between crack depth and resonant frequency. Three measurements of each crack are included in these results and the agreement in resonant frequency within each set of three shows that these measurements are repeatable with respect to probe position.

4.3. FINITE CRACKS

Figure 4.15 shows the resonant response for different crack lengths. Figure 4.15a shows the magnitude of reflection coefficient for six different finite-crack lengths. There is no significant change between the $L = a = 11$ mm and $L = 5$ mm curves. A small shift of the resonant frequency is seen for the $L = 4$ mm curve and the resonance continues to shift as the length becomes shorter, approaching the undamaged conducting plate case as the length goes to zero. Figure 4.15b shows the resonant frequency as a function of crack length. As observed from Figure 4.15a, there is no noticeable change for lengths greater

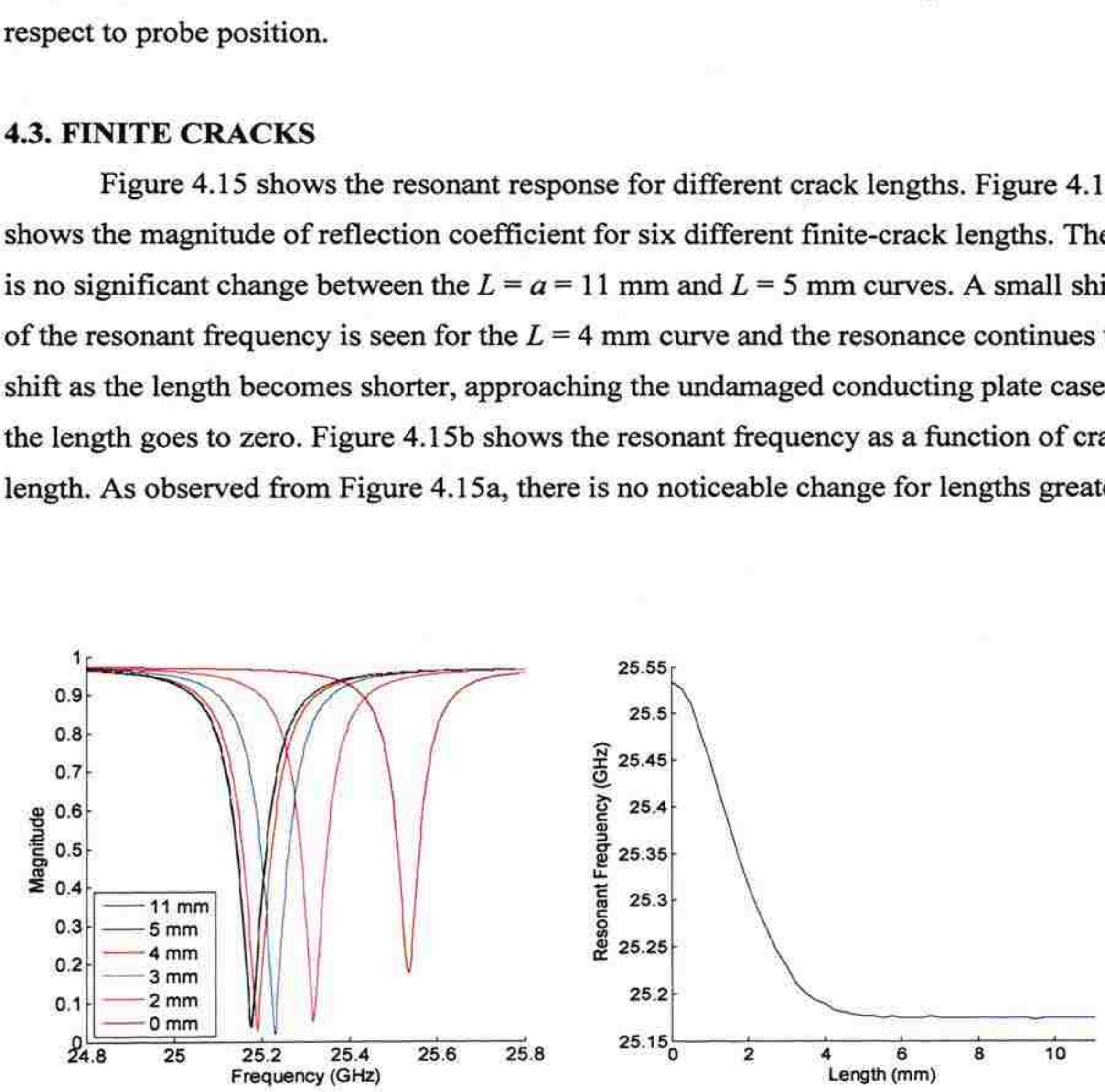

(a) (b)

Figure 4.15. Simulated resonant response for cracks in aluminum with $D = 0.2$ mm, $W = 0.5$ mm, and different lengths at K-band: a) magnitude of reflection coefficient as a function of frequency for six crack lengths and b) resonant frequency as a function of crack length.

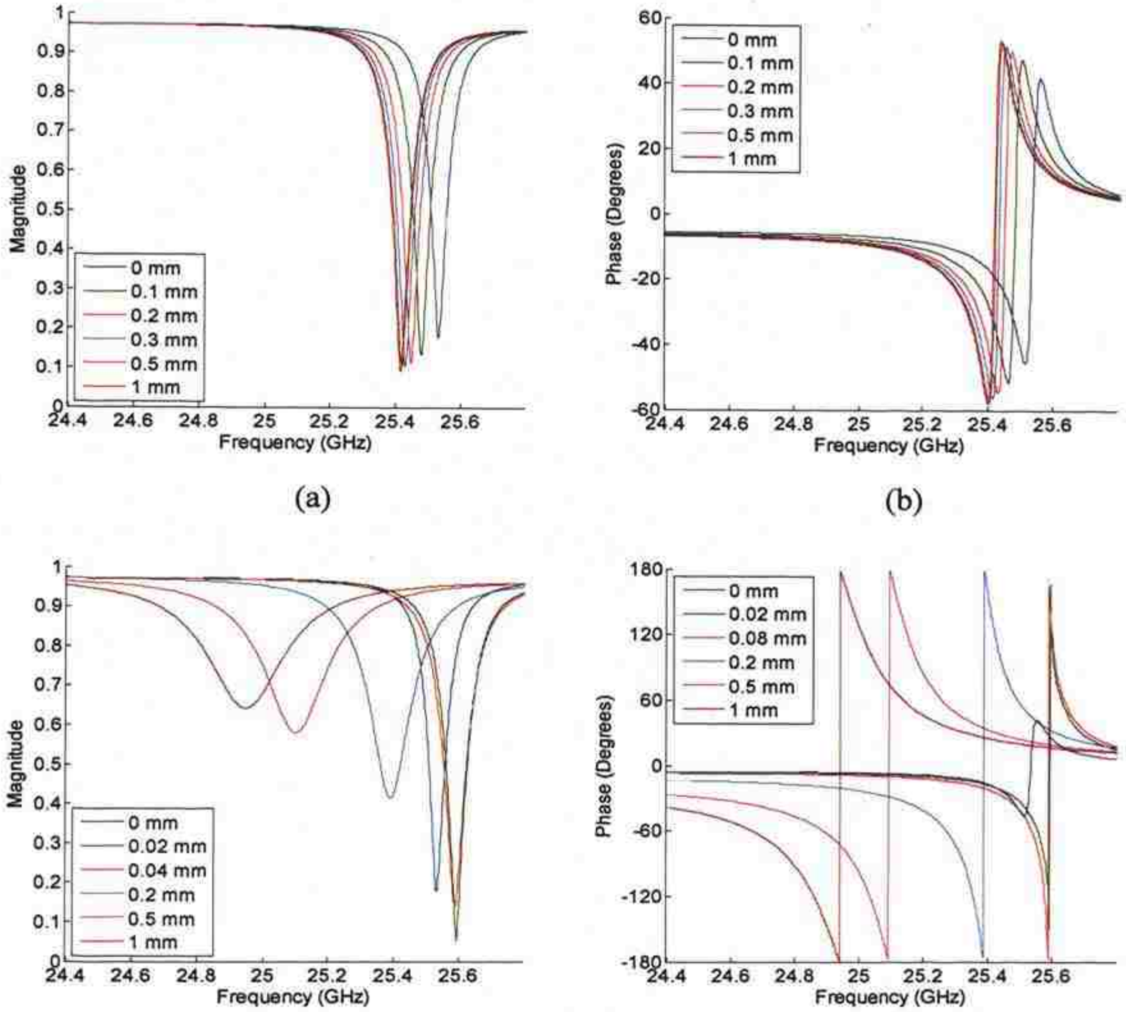

(a) (b)

(c) (d)

Figure 4.16. Simulated complex reflection coefficient as a function of frequency for pits in aluminum with two diameters and several depths at K-band: a) magnitude and b) phase for pits with diameter of 1 mm and six depths, and c) magnitude and d) phase for pits with diameter of 2 mm and six depths.

value as well, expected since they will only support non-propagating modes. The 1.5, 2, and 2.5 mm-diameter pits also each exhibit non-monotonic behavior with depth for the magnitude at resonance and/or the resonant frequency, as seen in Figures 4.17a-b. The non-monotonic behavior of the resonant frequency could introduce ambiguity in depth evaluation, as mentioned earlier. Figure 4.17c shows that for the 1.5, 2, and 2.5 mm-diameter pits the Q-factor drops as pit depth increases, with larger diameter pits also

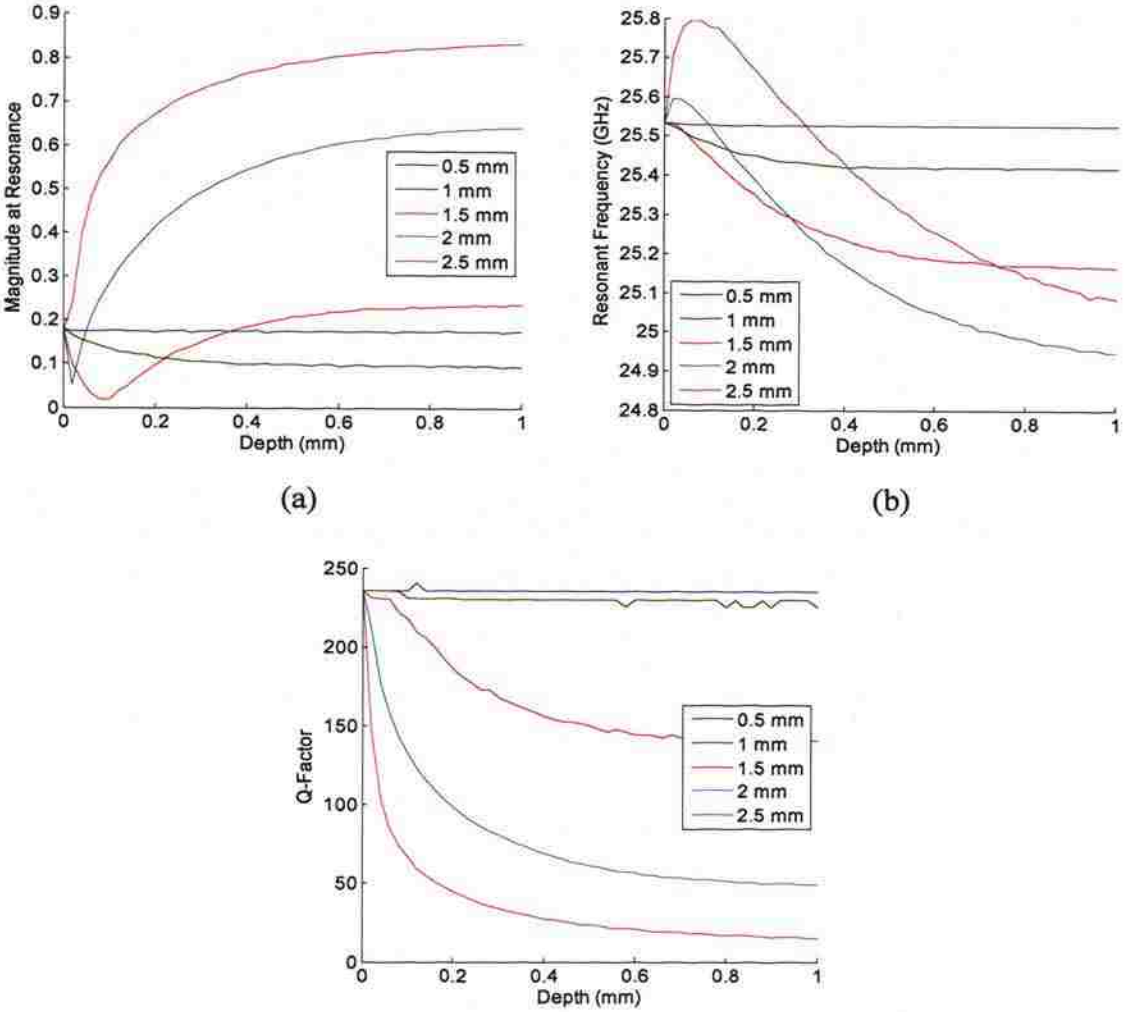

(a)

(b)

(c)

Figure 4.17. Simulated characteristics of resonant response as functions of depth for slab-loaded waveguide probe and pits with five diameters at K-band: a) magnitude at resonant frqeuency, b) resonant frequency, and c) *Q*-factor.

having lower *Q*-factors. It is also relatively large, around 230 if no pit is present (depth of zero); compared to a maximum of about 40 for both the empty and filled crack resonators.

Simulations including an offset of the pit 0.2 mm along *b* from the center of the waveguide showed that two resonances are observed (as for long cracks, see Figure 4.8), and furthermore that the behavior of these two resonances depends on pit diameter.

Figure 4.18 shows the magnitude and phase of reflection coefficient for offset pits with two different diameters, each with six different depths, at K-band. Figures 4.18a-b show that for 1 mm-diameter pits the depth shifts the resonant frequency, as in Figures 4.16a-b, but the shape of the resonant response is also distorted. This distortion is consistent with the interaction of two resonances with resonant frequencies very close to one another.

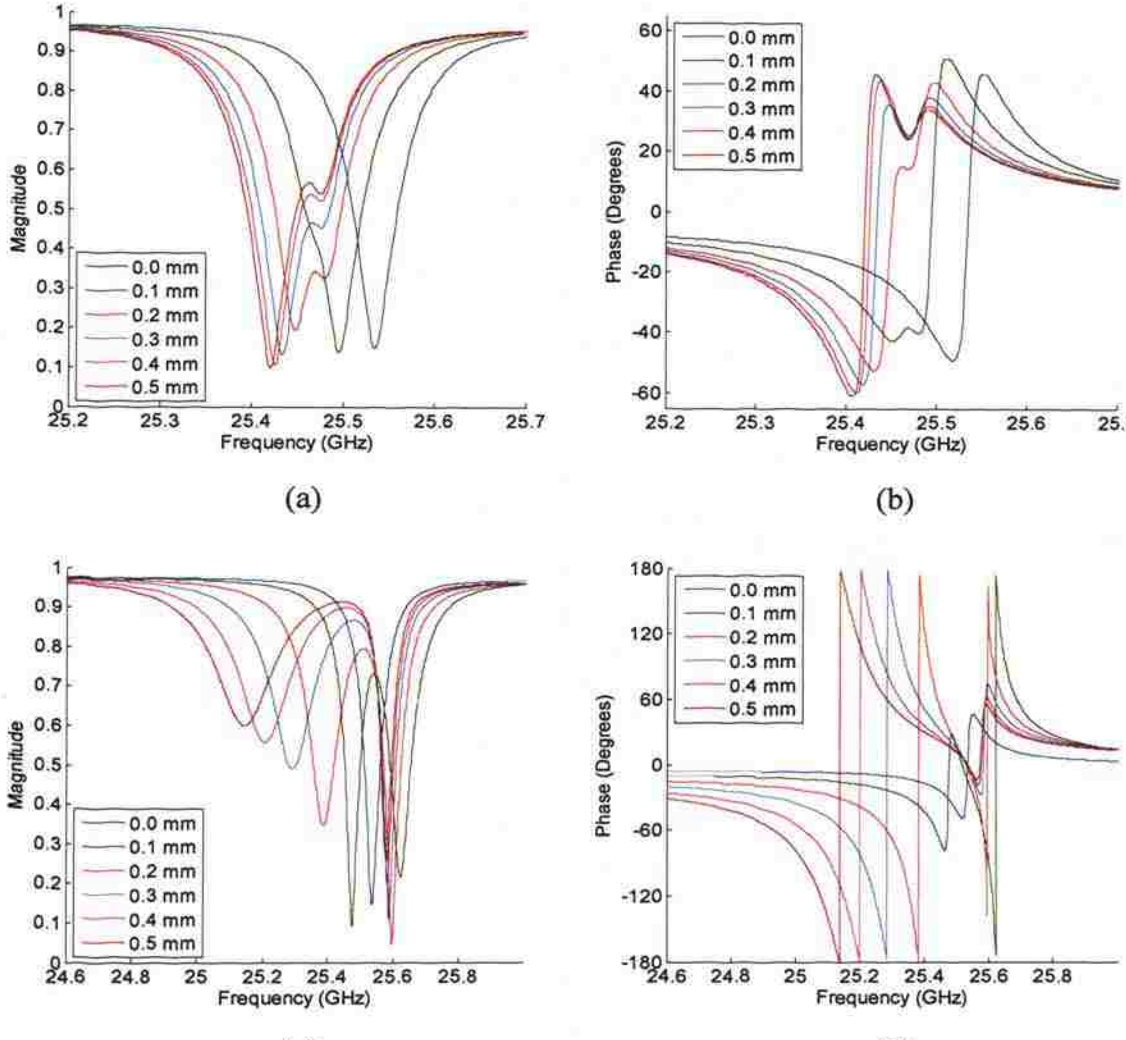

(a) (b)

(c) (d)

Figure 4.18. Simulated complex reflection coefficient as a function of frequency for pits in a perfect electric conductor with two diameters and six depths at K-band: a) magnitude and b) phase for pits with diameter of 1 mm and c) magnitude and d) phase for pits with diameter of 2 mm. Pits are offset 0.2 mm in the *b* direction from the center of the probe.

Figures 4.18c-d show that two resonant responses are observed for the offset pits with diameter of 2 mm. The resonant frequency of the leftmost (desired) resonance shifts significantly as a function of depth, but the rightmost resonance shifts very little. It is also worth noting that for both diameters the phase to the near-left of the resonances is ordered by depth.

Figure 4.19 shows the phase of reflection coefficient at a single frequency as a function of depth for pits with six diameters, including those in Figures 4.18b and d. Figure 4.19a shows that at 24.5 GHz the phase is clearly related to both depth and diameter for most of the pits. There is no change in the phase as a function of varying depth for the 0.5 mm-diameter pits, as was observed above, and the 1 mm-diameter pits seem to converge to a value around a depth of 0.3 mm. For any other combination of diameter and depth shown in this figure, depth can be uniquely identified using the phase information along with knowledge of the pit diameter. The curves are also sorted by diameter, and for the larger diameter pits the phase depends on depth in a near-linear fashion. Figure 4.19b shows the phase of reflection coefficient for similar conditions to Figure 4.19a, but at a measurement frequency of 25 GHz. A larger change in the phase is

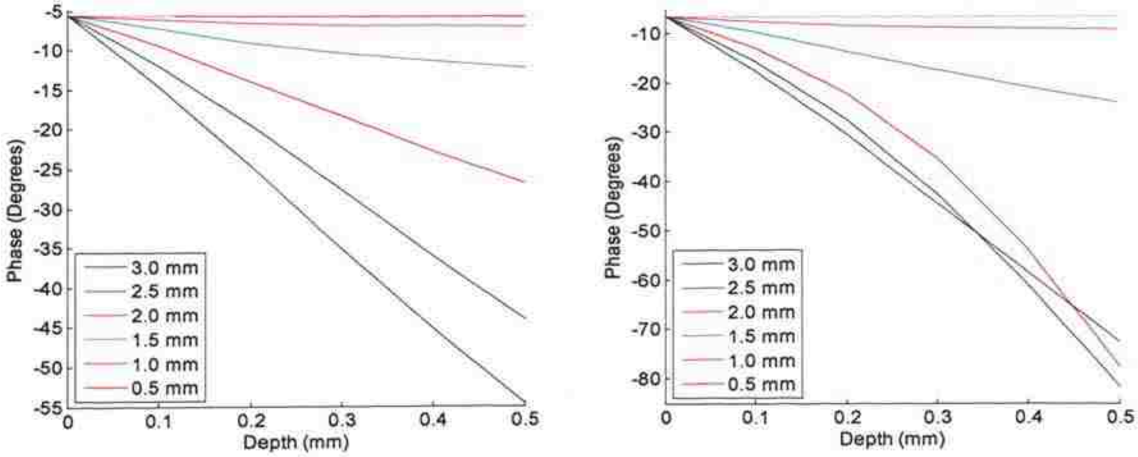

(a) (b)

Figure 4.19. Phase of reflection coefficient as a function of pit depth for pits in a perfect electric conductor with six diameters at two frequencies: a) 24.5 GHz and b) 25 GHz (K-band).

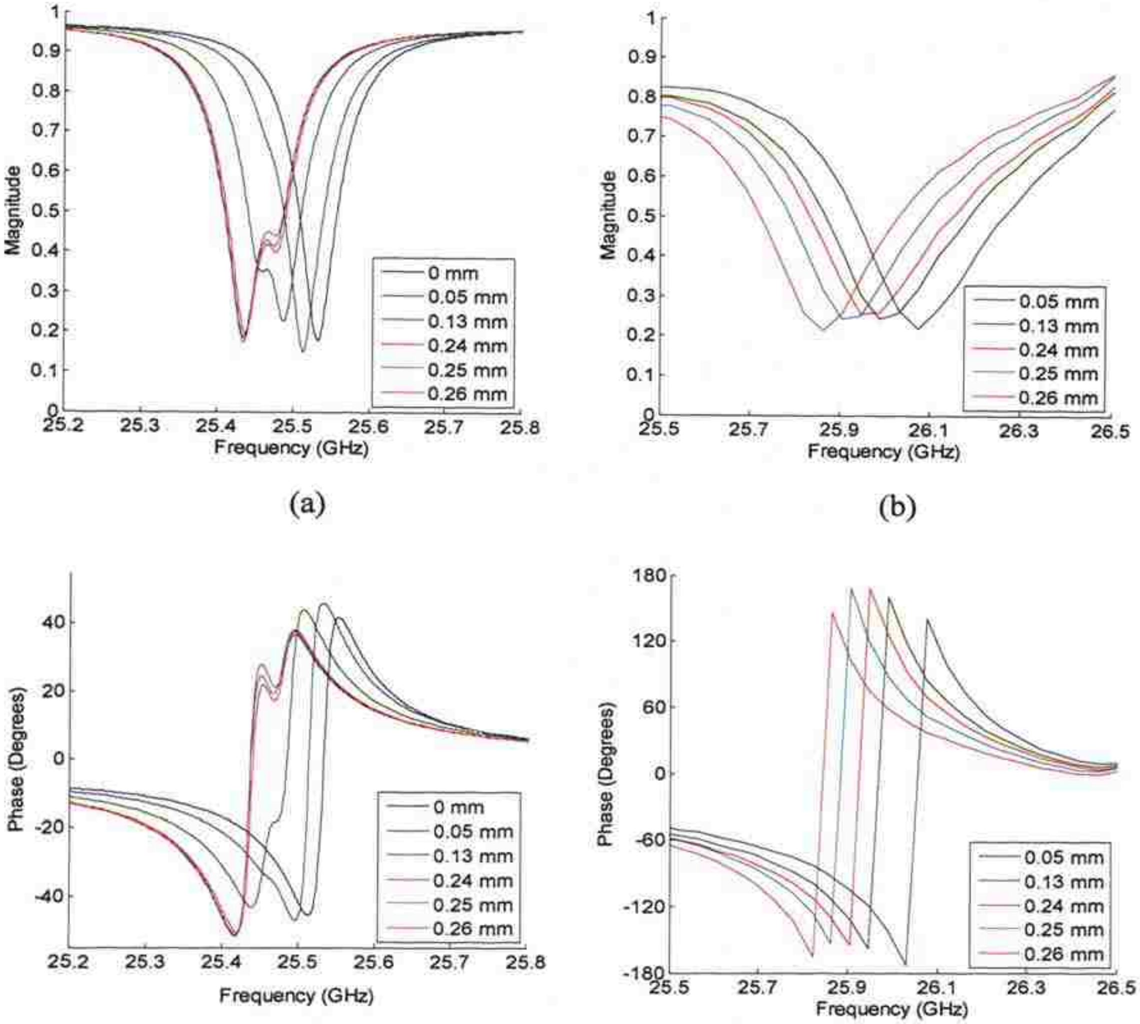

(a) (b)

(c) (d)

Figure 4.20. Complex reflection coefficient as a function of frequency for slab-loaded waveguide probe and pits in aluminum with diameter of 1.02 mm and five depths at K-band: a) simulated magnitude, b) measured magnitude, c) simulated phase, and d) measured phase. For the simulations the pits are offset 0.2 mm along *b* from the center of the waveguide and an undamaged (depth of zero) case is included for reference.

results shown in Figure 4.21a. Also, as for the 1.02 mm-diameter pits, only one resonance is seen in the measured results, but two are evident in the simulations. Again, this may indicate that the probe was very well positioned or that the second resonance is outside of the measured frequency band. A shift in the resonant frequency is observed which may be related to pit depth. Figures 4.20c-d show the simulated and measured phase for these

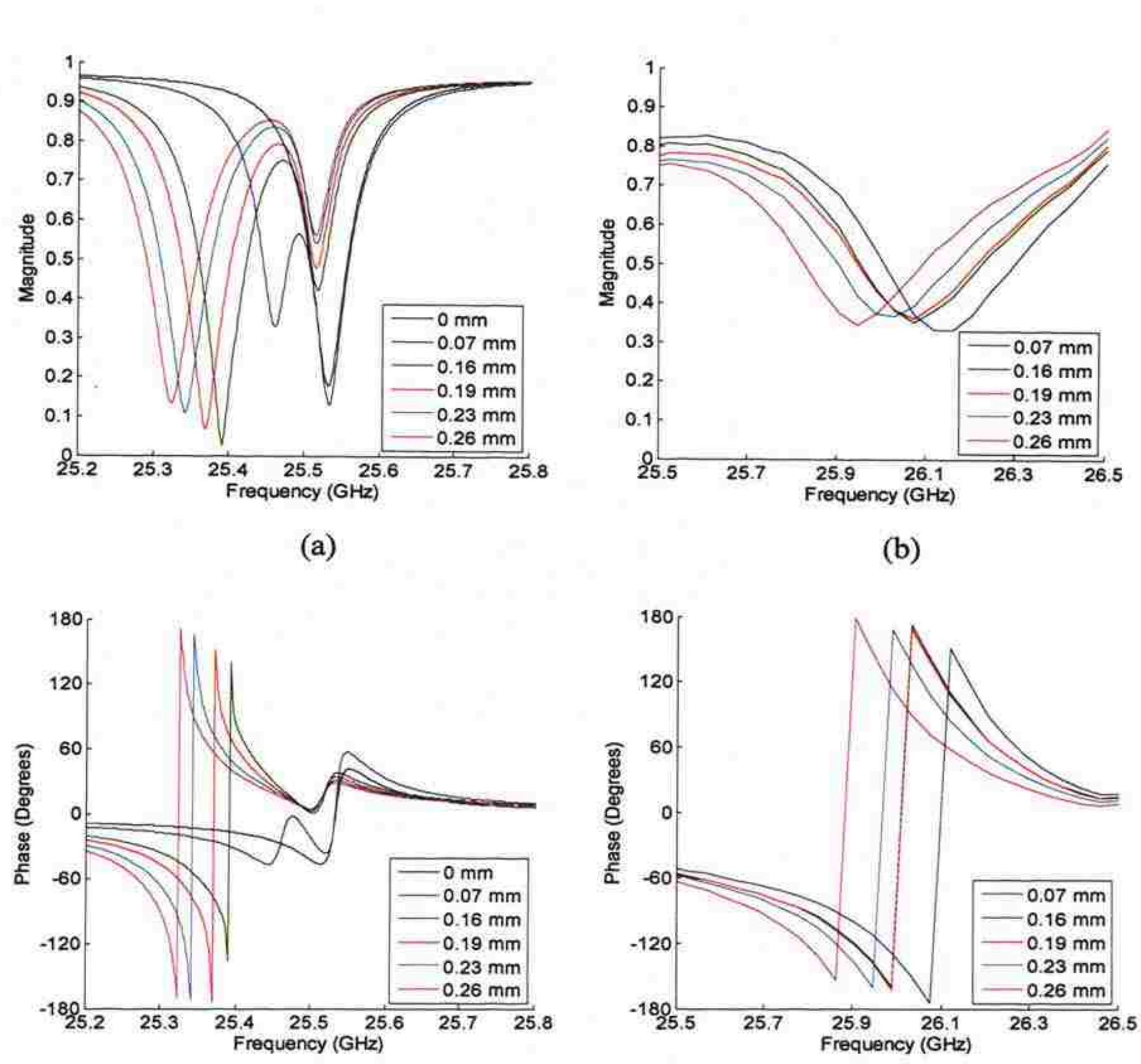

(a) (b)

(c) (d)

Figure 4.21. Complex reflection coefficient as a function of frequency for slab-loaded waveguide probe and pits in aluminum with diameter of 1.52 mm and five depths at K-band: a) simulated magnitude, b) measured magnitude, c) simulated phase, and d) measured phase. For the simulations the pits are offset 0.2 mm along *b* from the center of the waveguide.

pits. The simulations show that the first resonance is overcoupled and the second resonance in undercoupled (phase transitions of 360° and less than 360°, respectively). The measurement results show an overcoupled situation. The resonant frequencies indicated by the phase are in agreement with those indicated by their respective magnitude measurements. It is also noted that, once again, the phase to the left of the resonances is ordered by depth for both simulation and measurement.

Figure 4.22 shows the shift of the resonant frequency as a function of depth for the measurements (solid) and simulations (dashed) shown in Figures 4.20a-b and 4.21a-b. For each curve individually the shift is calculated relative to the shallowest pit. If the two deepest pit measurements of the 1.02 mm-diameter curve and the deepest measurement of the 1.52 mm-diameter curve are ignored, then a reasonable match is observed.

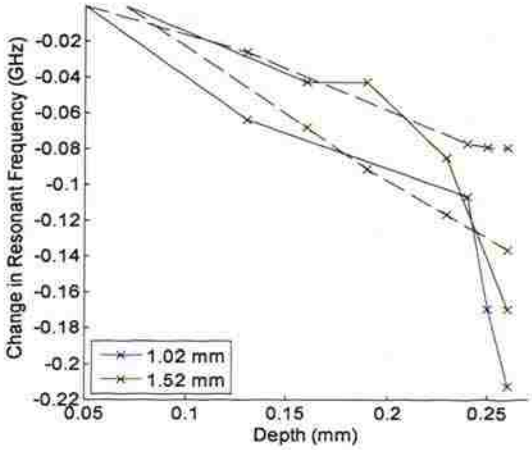

Figure 4.22. Measured (solid) and simulated (dashed) shift of resonant frequency as a function of depth (each curve referenced to its respective shallowest pit) for slab-loaded waveguide probe and pits in aluminum with two diameters at K-band.

A single-frequency phase measurement near the resonance, as shown for simulations in Figure 4.19a-b, may prove to be a more reliable approach for pits than evaluating the resonant frequency. Figure 4.23 shows the phase of reflection coefficient at 25.8 GHz for the measurements shown in Figures 4.20d and 4.21d as well as a set of pits with a diameter of 2.54 mm. Larger depths are clearly associated with greater changes in phase, with a significant change in phase even for small changes in depth. It is also interesting to note that for these measurements the larger diameter pits had a smaller overall change in phase for a similar change in depth, which is in contrast to the simulation results shown in Figure 4.19a. This reversal may be caused by the close proximity of the measurement frequency to the resonant frequency (consider Figure 4.19b, where the phase change is not fully ordered by diameter for the larger three pit diameters), the multiple resonance behavior of the pits, or some combination of the two.

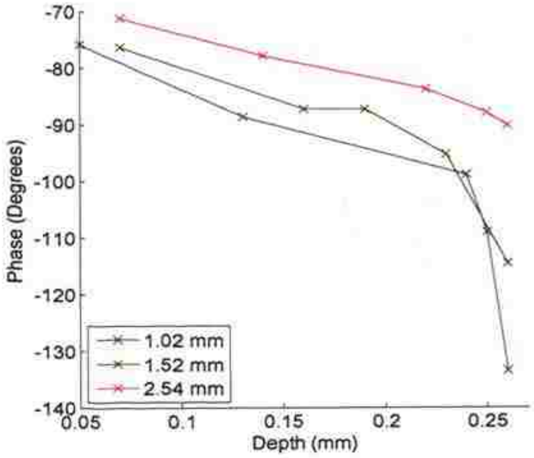

Figure 4.23. Measured phase of reflection coefficient at 25.8 GHz (near resonance) as a function of depth for pits in aluminum with three diameters at K-band.